DOE/PC/79916--7

DE90 003315

DETERMINATION OF LOCAL RADIATIVE PROPERTIES IN COAL-FIRED FLAMES

(Grant No: DE-FG22-87PC79916)

TECHNICAL PROGRESS REPORT - DOE/PC/79916-7

THE SECOND YEAR : 9/15/1988 - 9/15/1989

Submitted to the

U.S. Department of Energy
Pittsburgh Energy Technology Center

M. Pinar Mengüç

DISCLAIMER

DETERMINATION OF LOCAL RADIATIVE PROPERTIES IN COAL-FIRED FLAMES

(Grant No: DE-FG22-87PC79916)

TECHNICAL PROGRESS REPORT - DOE/PC/79916-6

SECOND YEAR - ANNUAL REPORT
SEPTEMBER 15, 1988 - SEPTEMBER 15, 1989

Submitted to the

U.S. Department of Energy
Pittsburgh Energy Technology Center

by

M. Pinar Mengüç (Associate Professor)

B. Agarwal (Graduate Student)
M. Bush (Graduate Student)
D. Dsa (Graduate Student)
S. Manickavasagam (Graduate Student)
S. Subramaniam (Graduate Student)

Department of Mechanical Engineering
University of Kentucky
Lexington, KY 40506-0046

PREFACE

This report summarizes the research performed on determining the radiative properties of coal particles under a grant from the U.S. Department of Energy Pittsburgh Energy Technology Center (Grant No: DE-FG22-87PC79916). The report covers the period September 15, 1988 through September 15, 1989.

During this period, three students completed their M.S. theses:

- Birendra M. Agarwal, Thesis title: "An Experimental and Theoretical Study of Single and Multiple Scattering in an Axisymmetric System", 1989.

(This research was primarily conducted under an NSF Grant No: CBT-8708679; however, the fundamentals developed here are to be used in our analytical and numerical studies in determining the coal radiative properties.)

- Shanker Subramaniam, Thesis title: "Solution of the Inverse Radiation Problem Using a Monte Carlo Technique", 1989.

(This research was partially supported by the University of Kentucky Center for Computational Sciences and the NSF Grant No: CBT-8708679.)

- Michael D. Bush, Thesis title: "A CO_2 Laser Nephelometer to Determine the Radiative Properties of Pulverized-Coal Particles", 1989.

1. INTRODUCTION

It is already known that the most important missing link in the prediction of radiation heat transfer in combustion systems is the lack of detailed information about the optical and physical properties of combustion products (Viskanta and Mengüç, 1987). Considering the uncertainty in the fundamental optical and physical properties of coal particles, such as complex index of refraction, size, size distribution, and shape, it is difficult to predict the radiative properties of particles using available analytical methods, such as the Lorenz-Mie theory or the extended boundary condition method. The reason we need to know the complex index of refraction and the size of the particles is to determine the radiative properties from theoretical models, which are good for homogeneous particles with well defined shapes. Even if have accurate values for the spectral complex index of refraction and size of the particles, a significant portion of that information will be lost because of the shape and concentration distribution approximations to be made. For a better understanding of radiation and radiation/combustion or radiation/turbulence interactions, it is preferable to determine the radiative properties *in situ*.

With these facts in mind, we proposed an "effective radiative property" concept for the particles in practical systems. These effective properties can be obtained from a detailed, interactive experimental/analytical procedure. First, a series of experiments are performed, and the attenuation and scattering of incident radiation at several angular orientations are recorded. The physical and optical characteristics of the total particle cloud determines the amount of attenuation, and this information is included in the measured projection data. Effective properties can be determined by solving the inverse radiation problem in a corresponding geometry using these projection intensity data as input. Following this, empirical relations for "effective radiative properties" can be derived for given physical conditions. This can be achieved if other physical properties, such as volume fraction and particle size distribution, temperature of the particles and combustion gases, and concentration distribution of gases can be predicted from theory or measured in parallel experiments, and their contributions to the experimental data are quantified.

In part (B), we discuss the experimental apparati developed to measure the radiative intensity distribution using a CO_2 laser nephelometer. Recently, we accomplished to have a uniform, steady flow of pulverized-coal particles in a slab-geometry. Also, we developed a very accurate calibration scheme using glass particles with known size and complex index of refraction.

2. RESEARCH PROGRESS

A. BASIC AND THEORETICAL STUDIES:

A-I. Inverse Analysis for Homogeneous Axisymmetric Systems

(Graduate Student: Birendra Agarwal)

We performed experiments and developed an inverse analysis for basic understanding of scattering of a collimated light source in homogeneous, cylindrical, participating media. In the experiments, we used mono- and polydisperse latex particle suspensions and a He–Ne laser. We included upto three orders of scattering in the analysis to be able to account for multiple scattering effects. Fig. 1 is to show the geometry and scattered intensity path considered in the analysis.

Because the particles we used in these experiments are homogeneous and spherical in shape, and because their optical properties are known, we can determine their radiative properties directly from the Lorenz-Mie theory. Using these properties, we predicted intensity distribution exiting the axisymmetric medium by solving the forward radiation problem. Then, we compared experimental results against the theory for different particles and medium optical thicknesses. Figs. 2 and 3, are the comparisons for monosize particles with diameters of 0.300 and 0.720 μm, respectively, which correspond to size parameter, $x=\pi d/\lambda$, of 2.0 and 4.8. In Figs. 4 and 5, comparisons are given for a cloud of polydispersions. In these figures, solid lines were obtained using four different mean diameters, and the experimental data were plotted four times. The results were normalized at 10°, to 1, 10, 100, and 1000, and the normalized intensity was given in logarithmic scale. Overall, agreement between the experiments and the theory is remarkably good. For polydispersions, three orders of successive scattering is sufficient to model intensity distribution

accurately. We could not find a significant effect of the choice of mean diameter on the results. However, we recommend using $d_{86}^{1/2}$ as the mean diameter to obtain the effective scattering diagram of particles, because it is the expression which appears in a theoretical model derived from the solution of the electromagnetic wave equation.

Using the experimental data, we attempted to recover the coefficients of the phase function of the polydispersions using four different approaches. The theory behind this analysis was given by Mengüç and Subramaniam (1989). The exact phase function coefficients and the percentage error in the recovered coefficients are shown in Tables 1 and 2 for monodispersions with d=0.300 μm and d=0.720 μm, respectively, and in Table 3 for polydispersed particle cloud. As it is seen from these tables, it is possible to recover the coefficients from the experiments accurately. The error in the first two recovered coefficients is usually less than 10%. That much error in the coefficients do not affect the accuracy of solution of the radiative transfer equation (Mengüç and Subramaniam, 1989).

The insight we gained from this study will be used in interpreting the results obtained from the cold-coal-flow and the pulverized-coal burner experiments. Details of this work has been discussed in a M.S. thesis by Birendra Agarwal, and a paper based on this work has been submitted for publication in the *International Journal of Heat and Mass Transfer*. This study has been funded mostly by the National Science Foundation, and partly by this DOE grant.

A-II. Inverse Monte-Carlo Techniques

(Graduate Student: Shanker Subramaniam)

We developed an inverse Monte-Carlo scheme to obtain phase function and absorption and scattering coefficient distributions in inhomogeneous layers. The geometry of the system considered is shown in Fig.6. This analysis can also be used if there is collimated radiation incident on the planar media, and it is especially useful for recovering the required radiative properties from cold-coal flow experiments.

We need a simple but accurate phase function approximation to employ in the inverse Monte

Carlo analyses. For this purpose, a step phase function approximation was introduced, and a paper based on this work was submitted and accepted for publication in the *Journal of Quantitative Spectroscopy and Radiative Transfer*. Fig. 7 shows a comparison of four different step-function approximations against the full Mie phase function for a 20–30 μm coal size distribution. Using this phase function in the inversion scheme, we recovered the single scattering albedo ω and the first coefficient of the phase function a_1; these results are depicted in Tables 4 and 5. Also shown in these tables is a comparison of the Monte Carlo and the exact F_N solutions of the forward radiation problem. In general, both the exact and inverse analyses based on the Monte Carlo technique yield very accurate results.

In Figs. 8, 9, and 10, we plot the recovered ω and a_1 parameters for $\tau = 0.1$, 1.0, and 2.0, respectively. In each figure, results from 20 different runs are shown. Because of the statistical nature of the Monte Carlo solution scheme, the results display statistical oscillations. For larger optical thicknesses, the amplitude of the oscillations is much smaller than that for $\tau = 0.1$. However, the average of results obtained from 20 runs yield accurate ω and a_1 values for all optical thicknesses. Note that, the results presented in these figures were obtained after introducing random error on the transmission and reflection readings. If the numerical experiments are repeated several times, the mean of the recovered results approach to exact values, even if there is 5 or 10% error in the transmission and back-scattered flux readings.

Details of this work are given in a M.S. thesis completed by Shanker Subramaniam. A paper based on this study was submitted for publication in the *International Journal of Heat and Mass Transfer*. Partial support for this phase of the work is obtained from University of Kentucky Center for Computational Studies and from the NSF grant.

A-III. Inverse Numerical Models

(Graduate Students: Sivakumar Manickavasagam)

In addition to stochastic inverse solution techniques, we are also developing deterministic inverse methods for both one-dimensional planar (see Figs. 11 and 12 for the nomenclature and

geometry) and two-dimensional axisymmetric media (see Fig. 1). Once the forward radiative transfer problem is formulated for either of these systems, the inverse problem can be obtained numerically using a least-square-fit technique. These models will also help us to evaluate the Monte Carlo technique.

In Table 6, we display the input parameters and those recovered from the numerical inversion technique for axisymmetric cylindrical systems. Here, we assumed the extinction coefficient β is constant, but the single scattering albedo ω is varying in the medium. Three different ω variations were considered. The inverse results agreed very well with the exact, input data. We also considered a problem with varying β and ω, and recovered these parameters assuming they have either a three- or four-step profiles. Fig. 13 shows the comparisons with the three-step profile. The agreement is again very good. Use of a finer discrete profile for recovering β or ω does not improve the results significantly.

A-IV. Tomographical Reconstruction

(Graduate Student: None)

Another inverse solution method we are working on is the tomographical reconstruction technique. We have developed two different mapping techniques for calculating the direct problem in axisymmetric, nonhomogeneous, single-scattering media, and they will be employed in the inverse solution. None of the available studies in the literature included scattering in the tomographical reconstruction analyses. Our work is unique in that respect, and can be used to recover both absorption and scattering coefficients in radially-inhomogeneous cylindrical media. Some results from this work will be reported in a later date.

B. EXPERIMETAL STUDIES:

B-I. Multiple-Wavelength Pyrometer Experiments

(Graduate Student: Mike Bush)

The multiple-wavelength pyrometer has been modified and it is now operational. This set up was used with the cold-coal flow experiments. Within next year, we will be using this set up to make more measurements. Fig. 14 shows the plan-view of the multiple-wavelength pyrometer. On Fig. 15, we plot the effective spectral extinction efficiency factor $Q_{e,\lambda}$ measured at five wavelengths. The repeatability of the experiments was not very good; however, we are working on the ways to solve this problem.

B-II. CO_2 Laser Light Scattering Experiments

(Graduate Students: Mike Bush, Darryl D'sa and M. Sivakumar)

We completed the experimental set up for the CO_2 laser. A special portable optical-table was built which can be fit next to both the pulverized-coal burner and cold-flow experimental set up. The detector tray was designed to house up to four detectors. The laser is focused on the flame, and the radiation at several different angles is recorded. This information is to be processed using one of the analytical inversion schemes described in Section A.

Fig. 16 depicts the plan-view of the CO_2-laser nephelometer and Fig. 17 is a schematic drawing of the optical platform and the data acquisition system. The visible wavelength He-Ne laser is primarily used for optical alignment purposes. Also shown on these figures is the optical platform which houses the optical rails, aperture stops and detectors. It is designed to be used for experiments with the pulverized-coal burner as well as with the cold-coal-flow system. This design has been tested in basic multiple scattering experiments (see section A-I) and has been proved to be efficient.

Calibration of the CO_2-Laser Nephelometer Detectors

Calibration of the detectors of the CO_2 laser nephelometer was done by using large size glass particles received from *Potter Industries*. Size distribution of the glass particles determined from the electron-microscope pictures (see Fig.18). A test cell was designed to obtain a one-dimensional homogeneous glass-particle flow. Schematic of calibration system is depicted in Fig. 19. The glass-particle test cell was placed on a mount above the burner; therefore, once the detectors are

calibrated with this system, they can be used for the burner experiments. For the cold-coal-flow experiments, we needed to mount the coal test cell after completing the calibration.

The scattering measurements were performed between 6° and 15° for the glass particles. Before 6°, no data can be collected because of the blockage of radiation by the detector mounts and because of the inseparable effect of transmitted light from the scattered intensity data. After 15°, the scattered intensity level was too low to to be detected accurately.

The comparison of the experimental and theoretical results for the intensity distribution is given in Fig. 20. Here, the solid line is the theoretical result based on the first-order theory. The dashed line includes both first and second order scattering effects. These results are normalized with respect to the power of the incident radiation. The experimental results are obtained in units of millivolts. A calibration factor can be obtained by matching theoretical results with the experimental values. From the particular data presented calibration factor K was found to be equal to 0.16. Also found was an angular shift in the recording, which was because of the orientation of laser beam with respect to glass flow. This shift, which was less than 1°, detected because the theoretical and experimental peaks and dips did not match exactly. Using this information, calibration was also done angularly.

After the detectors of the CO_2-laser nephelometer were calibrated, we performed experiments with the coal particles. For this study we used Kentucky #9 coal as received from the Department of Energy Penn State Data Base. The proximate and ultimate analyses of coal as received and after completing the classification are shown in Tables 7 and 8. The size distribution of the size-graded coals were performed using electron microscope pictures. The area of different coal particles were measured and then a mean diameter based on d^8/d^6 was obtained. In Figs. 21 and 22, the size distribution of 15-35 μm and 45-65 μm coal particles are shown.

Using these coal particles, we measured scattering intensity distribution from cold-coal-flow test cell. The results are depicted in Fig. 23. The small size particles displayed a less steeper drop in the phase function values compared to 45–65 μm coals. Another important point to note on this figure is the repeatability of the experiments. Two different experimental sets obtained with

15–35 μm coal particles yielded almost identical results. We also performed experiments in the burner and recorded the angular intensity distribution at two different flame heights. As seen from Fig. 23, the effective scattering characteristics of coal particles change significantly as the coal particles burn, yet no change is observed after 14°.

B-III. Narrow Band Transmission/Scattering Experiments

(Graduate Students: Darryl D'sa and M. Sivakumar)

Scattering and transmission experiments will also be conducted in the 0.6-1.9 μm range using a Mercury–arc lamp and a monochromator. To be able to focus the light to a very small area and to use photomultiplier (PM) tubes for detection, the narrow-band spectral light from the monochromator will be transmitted using fiber optic probes. For this arrangement, a new set of optical rails and a mount to couple probes with the PM tubes are needed. For this purpose, a detector housing and optical rails was designed and construction is under way. Experimental results using this system will not be available probably before the end of the year.

3. SUMMARY AND FUTURE WORK

During the second year, we have completed most of the theoretical models required in this study. Also, we completed the test-cells to be used in the experiments. A limited number of experiments were performed with Kentucky #9 coal.

Three M.S. thesis have already been completed (by Agarwal, Bush and Subramaniam). The fourth M.S thesis (by D'sa) will be finished in early Summer 1990, and a Ph.D. dissertation (by Manickavasagam) is expected to be completed in 1991. These works put mile stones to the research, because each of them represents one completed aspect of the problem.

Within the next year, we will make the measurements with several different coals using both the cold-coal-flow system and the burner. We are working on installing a computer-controlled turntable to our CO_2-laser nephelometer. This will allow us to make more accurate experiments and have more reliable data from different coals. In addition to these, we are planning to change

the temperature of coal particles in cold-flow test cell to investigate the effect of temperature dependence on the effective radiative properties. Also, we will work on different theoretical models next year, including tomographical reconstruction, Monte-Carlo analysis for cylindrical systems, and discrete-dipole method to determine radiative properties of irregular-shaped particles.

4. REFERENCES

Viskanta, R. and Mengüç, M.P., 1987, "Radiation Heat Transfer in Combustion Systems", *Progress in Energy and Combustion Science,* Vol. 13, pp.97-160.

Mengüç, M.P. and Subramaniam, S., 1989, "A Step Function Approximation for the Experimental Determination of the Effective Scattering Phase Function of Particles", *Journal of Quantitative Spectroscopy and Radiative Transfer,* in press.

TABLE 1

Percentage error in the coefficients of the Legendre polynomial expansion of the phase function recovered from the experiments. Monodispersed particles with $d = 0.300\mu m$. Fourth order B-spline was fitted to 15 observation points. Bessel function fit was for $\theta < 10^o$.

	A COEFFICIENTS	ERROR IN THE COEFFICIENTS USING	
		B-SPLINE FIT	BESSEL FUNCTION
1	0.196007E+01	1.81	3.64
2	0.147085E+01	6.11	10.14
3	0.681389E+00	12.04	24.06
4	0.226122E+00	29.39	75.14
5	0.485373E-01		
6	0.693936E-02		
7	0.700315E-03		
8	0.524709E-04		
9	0.302982E-05		

TABLE 2

Percentage error in the coefficients of the Legendre polynomial expansion of the phase function recovered from the experiments. Monodispersed particles with $d = 0.720\mu m$. Fourth order B-spline was fitted to 15 observation points. Bessel function fit was for $\theta < 10^o$.

	A COEFFICIENTS	ERROR IN THE COEFFICIENTS USING			
		B-SPLINE FIT	BESSEL FUNCTION	STEP FUNCTION	DELTA FUNCTION
1	0.266106E+01	-0.25	0.37	-0.65	-11.24
2	0.372790E+01	-1.01	-0.29	-2.01	-11.85
3	0.414407E+01	-2.89	-1.99	-4.76	-13.21
4	0.394696E+01	-5.14	-3.94	-8.27	-14.33
5	0.332291E+01	-7.24	-5.55	-12.15	-13.97
6	0.241468E+01	-7.33	-4.66	-15.08	-8.32
7	0.140533E+01	-5.12	0.03	-18.68	11.14
8	0.657514E+00	-2.57	9.45	-27.64	74.83
9	0.240345E+00	-16.15	19.12	-62.74	321.71
10	0.704893E-01				
11	0.167702E-01				
12	0.328864E-02				
13	0.540453E-03				
14	0.755492E-04				
15	0.908918E-05				

TABLE 3

Percentage error in the coefficients of the Legendre polynomial expansion of the phase function recovered from the experiments. Polydispersed particles; $\overline{d} = d_{10}$. Fourth order B-spline was fitted to 15 observation points. Bessel function fit was for $\theta < 10^o$.

	A COEFFICIENTS	ERROR IN THE COEFFICIENTS USING			
		B-SPLINE FIT	BESSEL FUNCTION	STEP FUNCTION	DELTA FUNCTION
1	0.273638E+01	-1.83	-4.01	-3.27	-3.79
2	0.402291E+01	-5.63	-8.07	-9.23	-9.70
3	0.479925E+01	-9.85	-12.69	-16.27	-16.69
4	0.509409E+01	-14.23	-17.61	-24.20	-24.54
5	0.497523E+01	-16.91	-21.04	-31.13	-31.36
6	0.453870E+01	-18.69	-23.90	-38.36	-38.45
7	0.383758E+01	-18.22	-25.12	-45.50	-45.37
8	0.301025E+01	-16.44	-26.05	-55.13	-54.59
9	0.215717E+01	-10.36	-24.75	-67.46	-66.15
10	0.131744E+01	7.75	-17.13	-86.99	-83.87
11	0.646407E+00	66.20	13.43	-120.19	-111.80
12	0.264055E+00				
13	0.874847E-01				
14	0.241029E-01				
15	0.561123E-02				
16	0.112222E-02				
17	0.195558E-03				
18	0.300310E-04				
19	0.409906E-05				

Table 4: Direct and Inverse Monte Carlo Results

With Step-Isotropic Approximation for 6 Term Phase Function.
Direct F_N Results [1-Q(0)]=0.76057, Q(1)=0.45588
$\omega = 0.8$, $a_1 = 0.6438$, $\tau_0 = 1$, $n = 10$, $N = 50,000$

		Direct Results		Inverse Results		
$\Delta\theta$	Seed	1-Q(0)	Q(1)	ω	a_1	NI
10	I	0.7631	0.4572	0.801	0.616	21
	II	0.7692	0.4553	0.807	0.585	21
20	I	0.7605	0.4569	0.800	0.637	22
	II	0.7629	0.4602	0.805	0.596	21
30	I	0.7607	0.4564	0.800	0.639	22
	II	0.7630	0.4588	0.805	0.604	21
40	I	0.7600	0.4566	0.799	0.642	22
	II	0.7622	0.4582	0.805	0.614	21
50	I	0.7604	0.4561	0.799	0.643	22
	II	0.7619	0.4583	0.804	0.615	22
60	I	0.7603	0.4558	0.798	0.646	22
	II	0.7615	0.4588	0.802	0.615	22

NI Number of Iterations
I Seed 34567
II Seed 76543

Table 5: Direct and Inverse Monte Carlo Results

With Step-Isotropic Approximation for 25 Term Phase Function.
Direct F_N Results [1-Q(0)]=0.94178, Q(1)=0.63874
$\omega = 0.8$, $a_1 = 2.6028$, $\tau_0 = 1$, $n = 10$, $N = 50,000$

		Direct Results		Inverse Results		
$\Delta\theta$	Seed	1-Q(0)	Q(1)	ω	a_1	NI
10	I	0.9442	0.6486	0.794	2.574	15
	II	0.9405	0.6808	0.794	2.562	16
20	I	0.9417	0.6377	0.794	2.605	15
	II	0.9426	0.6393	0.795	2.597	16
30	I	0.9392	0.6345	0.796	2.626	18
	II	0.9391	0.6311	0.799	2.632	18
40	I	0.9336	0.6333	0.795	2.646	14
	II	0.9373	0.6335	0.800	2.642	17

NI Number of Iterations
I Seed 34567
II Seed 76543

TABLE 6 Comparisons of the input and recovered extinction coefficient and the single-scattering albedo values for three cases. Variable albedo, constant beta.

DISCRETE - W
****

	INPUT *****	RECOVERED *********
0.0000 < R < 0.3333	0.8000000000	0.8000000000
0.3333 < R < 0.6667	0.5000000000	0.5000000000
0.6667 < R < 1.0000	0.2000000000	0.2000000000

THE EXTINCTION COEFFICIENT
************** ************

INPUT *****	RECOVERED *********
0.8000000000	0.8000000000

DISCRETE - W
****

	INPUT *****	RECOVERED *********
0.0000 < R < 0.2500	0.9000000000	0.9000000000
0.2500 < R < 0.5000	0.7000000000	0.7000000000
0.5000 < R < 0.7500	0.5000000000	0.5000000000
0.7500 < R < 1.0000	0.3000000000	0.3000000000

THE EXTINCTION COEFFICIENT
************** ************

INPUT *****	RECOVERED *********
0.8000000000	0.8000000000

CONTINUOUS - W
****
THE CONSTANTS IN A*R**2 + B*R + C ARE DETERMINED

INPUT *****	RECOVERED *********
1.0000000000	1.0000000000
-1.0000000000	-1.0000000000
0.8000000000	0.8000000000

THE EXTINCTION COEFFICIENT
************** ************

INPUT *****	RECOVERED *********
0.8000000000	0.8000000000

TABLE 7 Coal Analysis as received for Kentucky #9 HVA Bituminous Coal

Proximate Analysis (as received)	Weight Percent	Ultimate Analysis (dry)	Weight Percent
Moisture	6.88	C	63.24
Volatile Matter	38.20	H	5.11
Fixed Carbon	44.10	S	4.03
Ash	10.82	N	1.22
		Ash	26.40
Total	100.00	Total	100.00
Heating Value (dry)		26,540 kJ/kg	

TABLE 8 Size-graded Coal Analysis (weight %)
Kentucky #9 HVA Bituminous Coal

Coal Size	15-35 μm	45-65 μm
Proximate Analysis		
Moisture	3.20	3.71
Volatile Matter	38.90	39.00
Fixed Carbon	49.28	47.10
Ash	8.62	10.19
Total	100.00	100.00
Ultimate Analysis (dry)		
C	68.69	65.99
H	5.09	4.90
N	1.34	1.35
S	3.96	4.84
O	8.79	8.12
Ash	12.13	14.80
Total	100.00	100.00
Heating value (kJ/kg, dry)	31,820	32,220

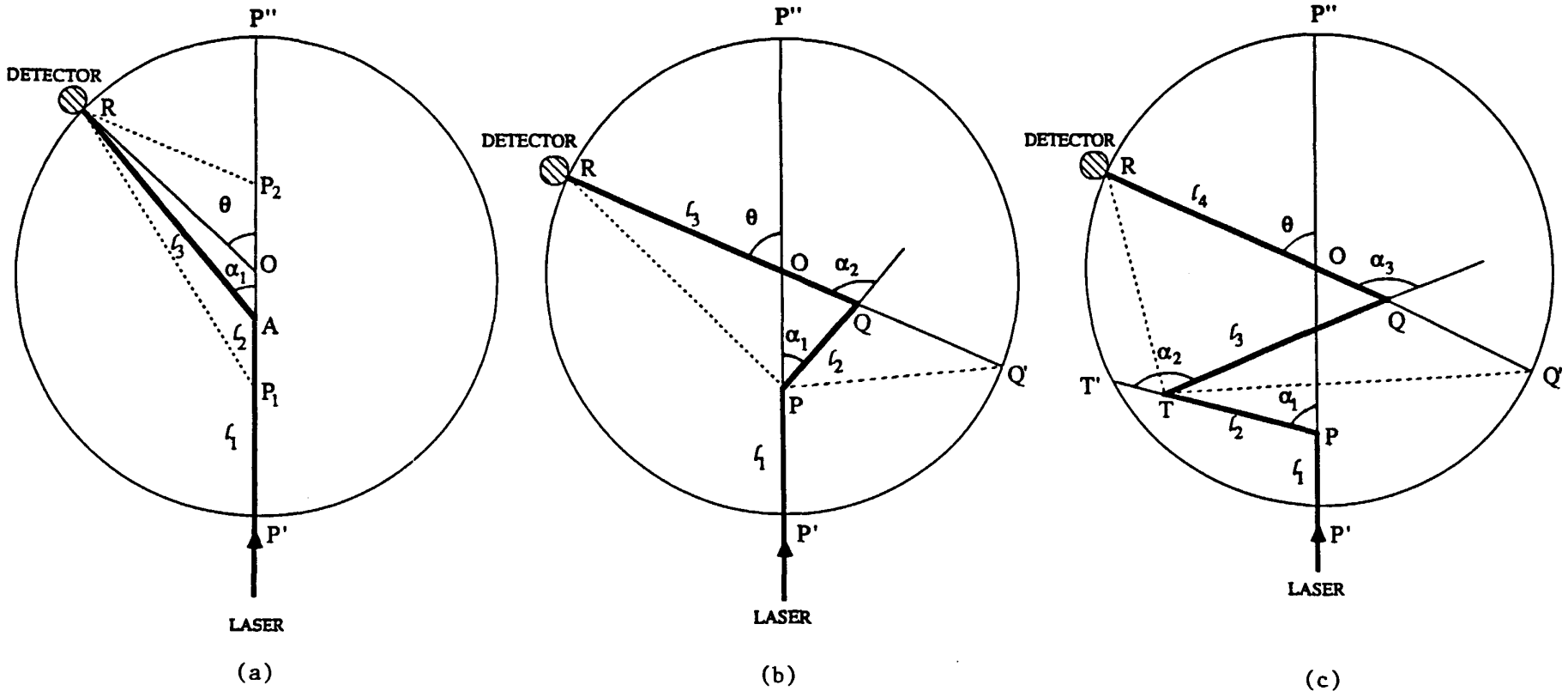

FIGURE 1 First (a), second (b), and third (c) order scattering of laser radiation in homogeneous cylindrical medium.

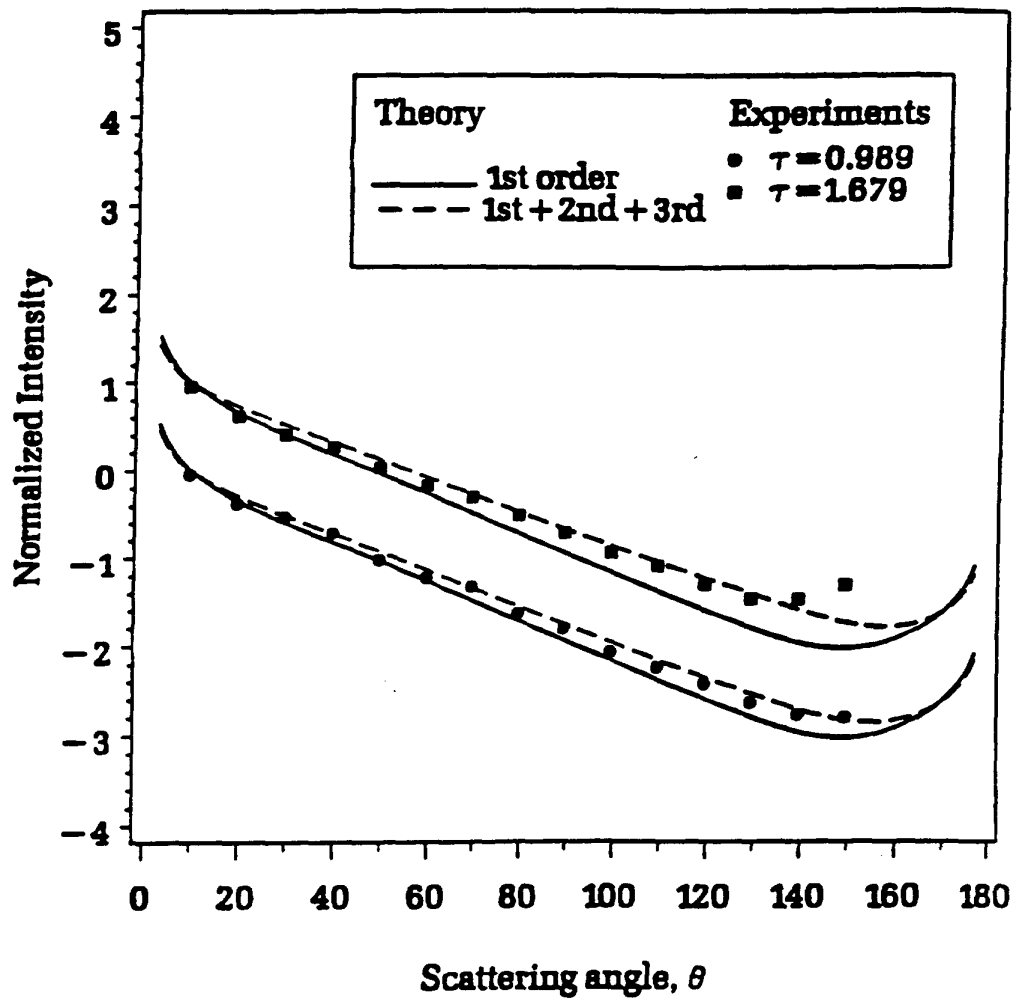

FIGURE 2

Normalized angular intensity distribution for monodispersed particles; $d = 0.300\ \mu m$. Points are the experimental data and lines are the theoretical predictions. Results are normalized at 10^o to 1, 10, 100, with increasing τ, respectively.

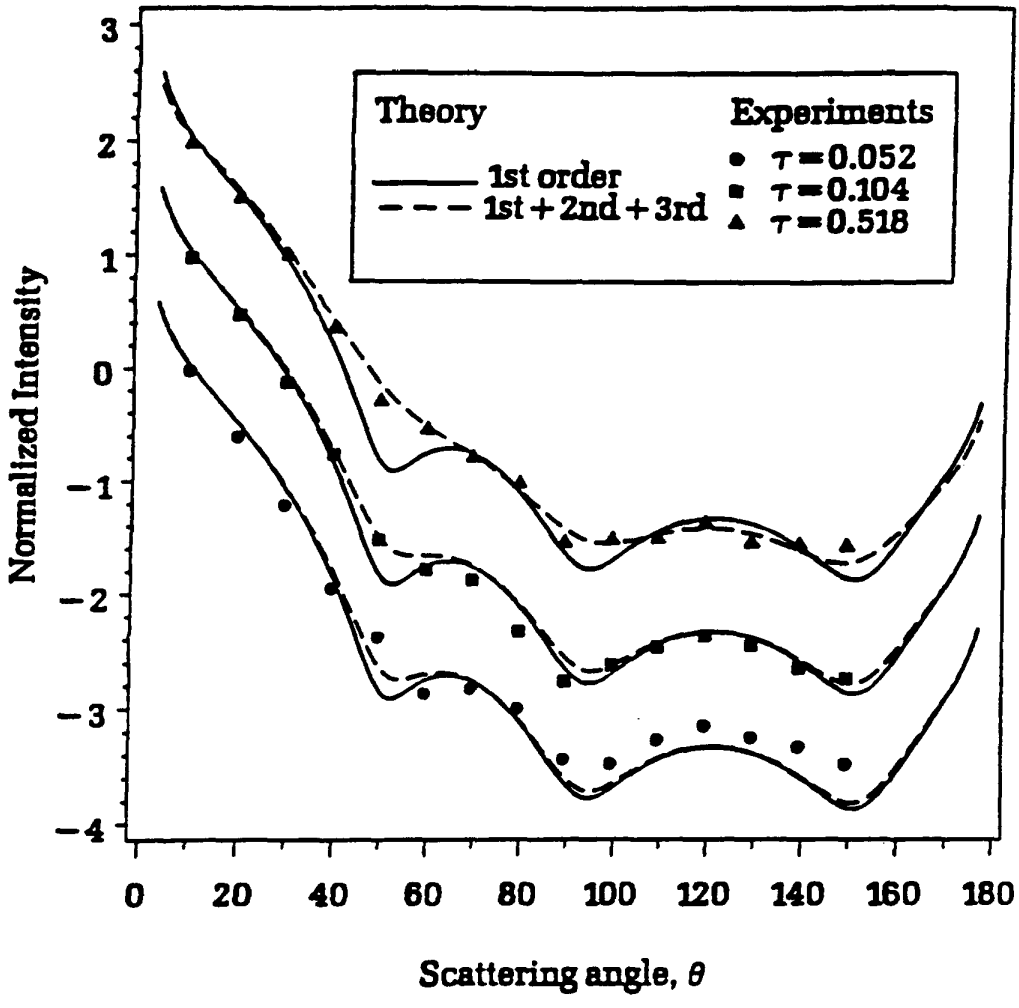

FIGURE 3

Normalized angular intensity distribution for monodispersed particles; $d = 0.720\ \mu m$. Points are the experimental data and lines are the theoretical predictions. Results are normalized at 10^o to 1, 10, 100, with increasing τ, respectively.

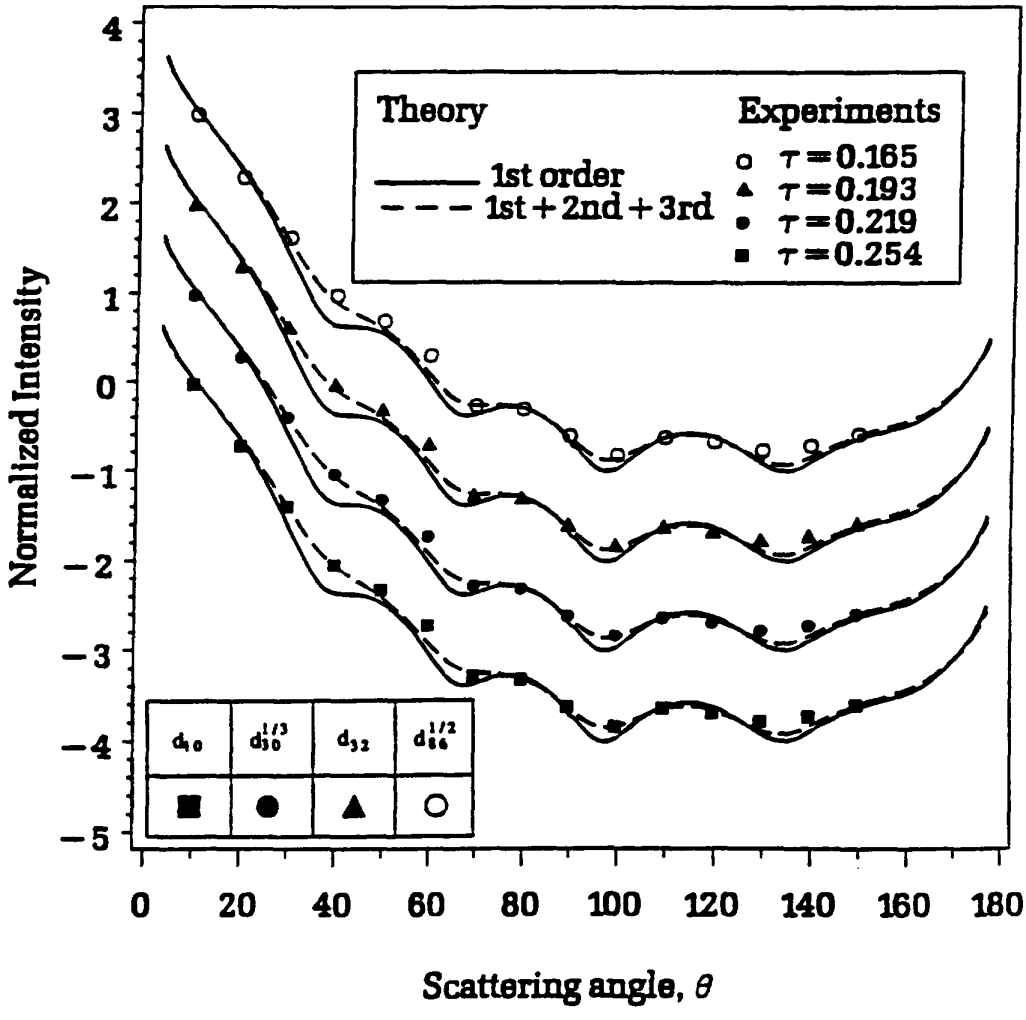

FIGURE 4

Normalized angular intensity distribution for polydispersed particles. Points are the experimental data (same for all four plots) and lines are the theoretical predictions Comparisons for $\tau < 0.15$.

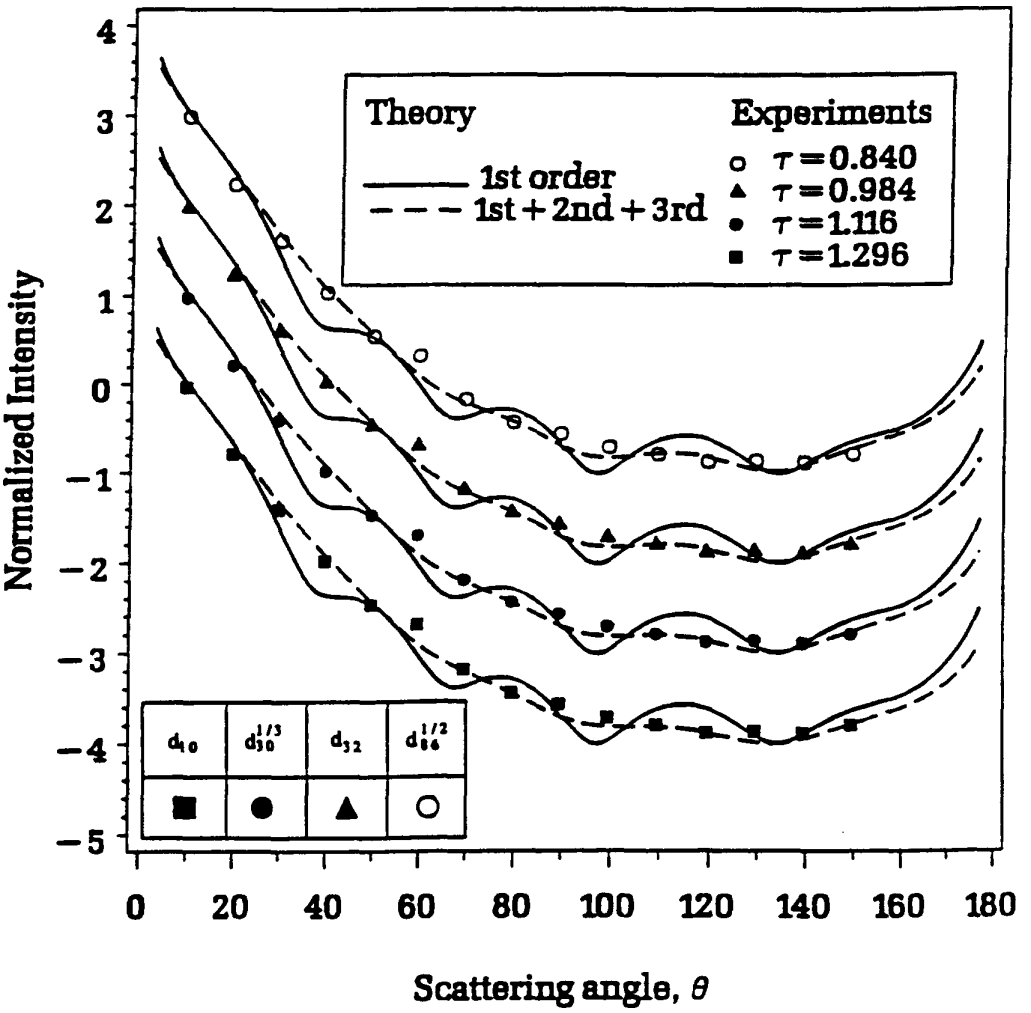

FIGURE 5

Same as Fig. 4. Comparisons for $0.8 < \tau < 1.3$.

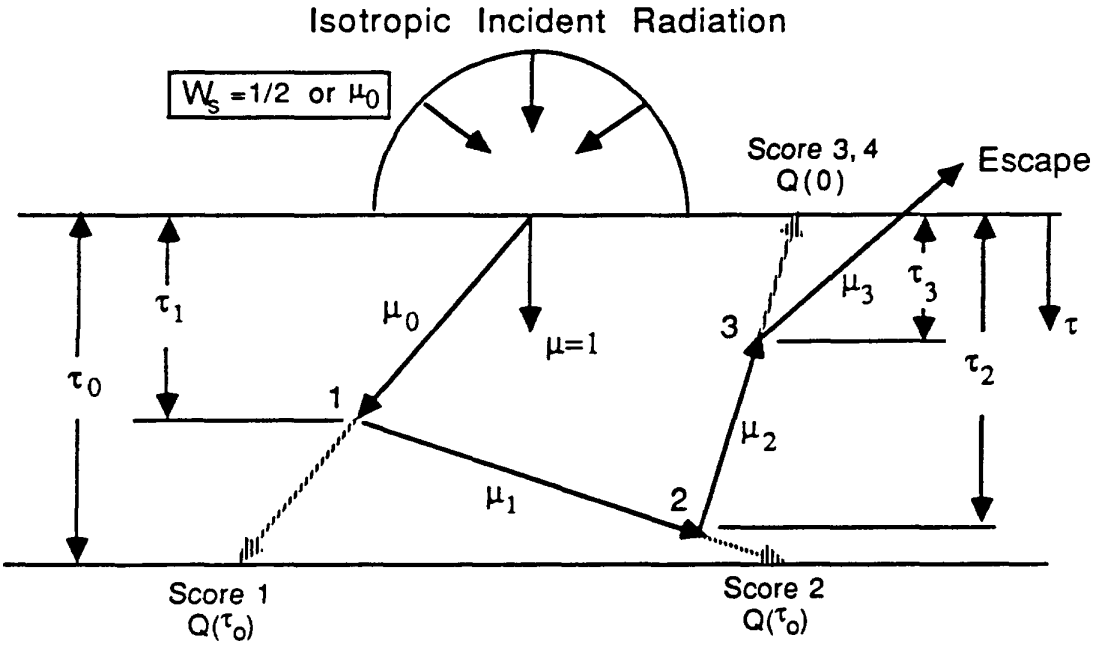

FIGURE 6

The last flight estimation for a photon with 3 scatters before escape. LFE extensions shown as the dashed lines.

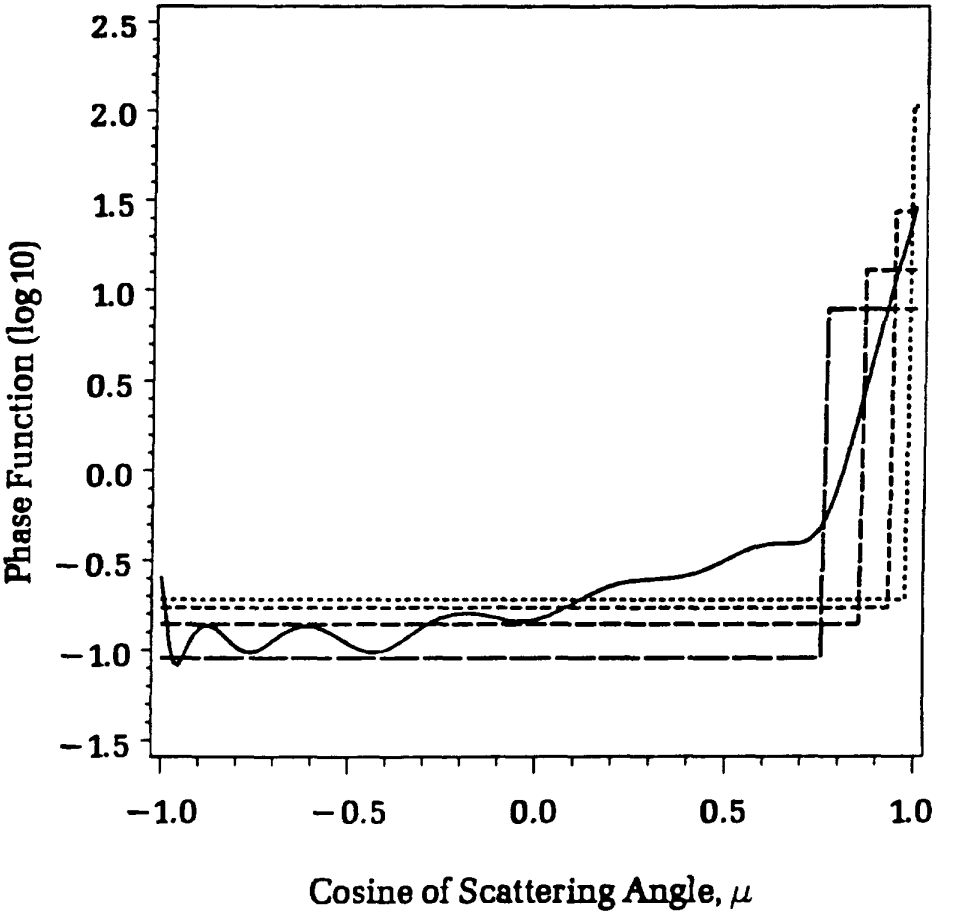

FIGURE 7

Phase function for pulverized-coal size distribution.
Exact results (solid line) from Lorenz-Mie theory (19 term).
Step approximations with 10, 20, 30, and 40 degrees for the forward step.

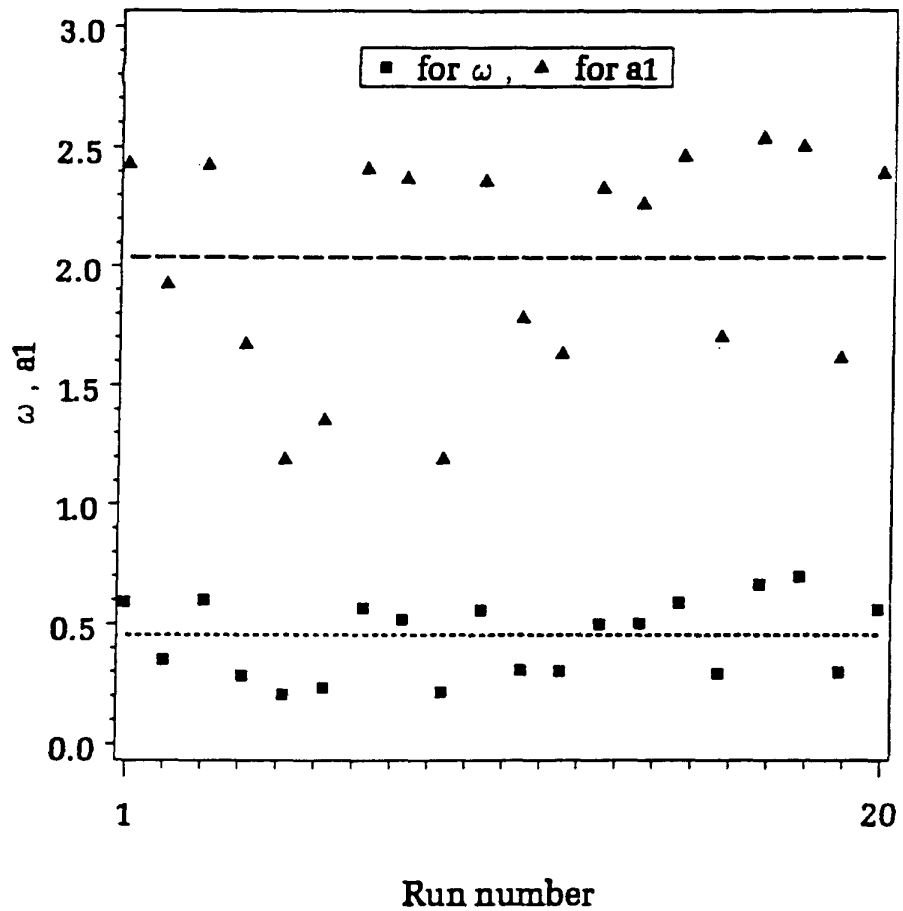

FIGURE 8

Inverse results for the single scattering albedo and the first coefficient of the phase function expansion, and the mean values. The exact values are $\tau_0 = 0.1$, $\omega = 0.5$, and and $a_1 = 2.409$ (PF-1). Random errors are within $\pm 10\%$ for $Q(0)$ and $\pm 5\%$ for $Q(1)$. Converged values without error are $\omega = 0.497$ and $a_1 = 2.278$. The upper bounds are ± 0.389 for $\hat{\omega}$ and ± 8.252 for $\hat{a}_1$.

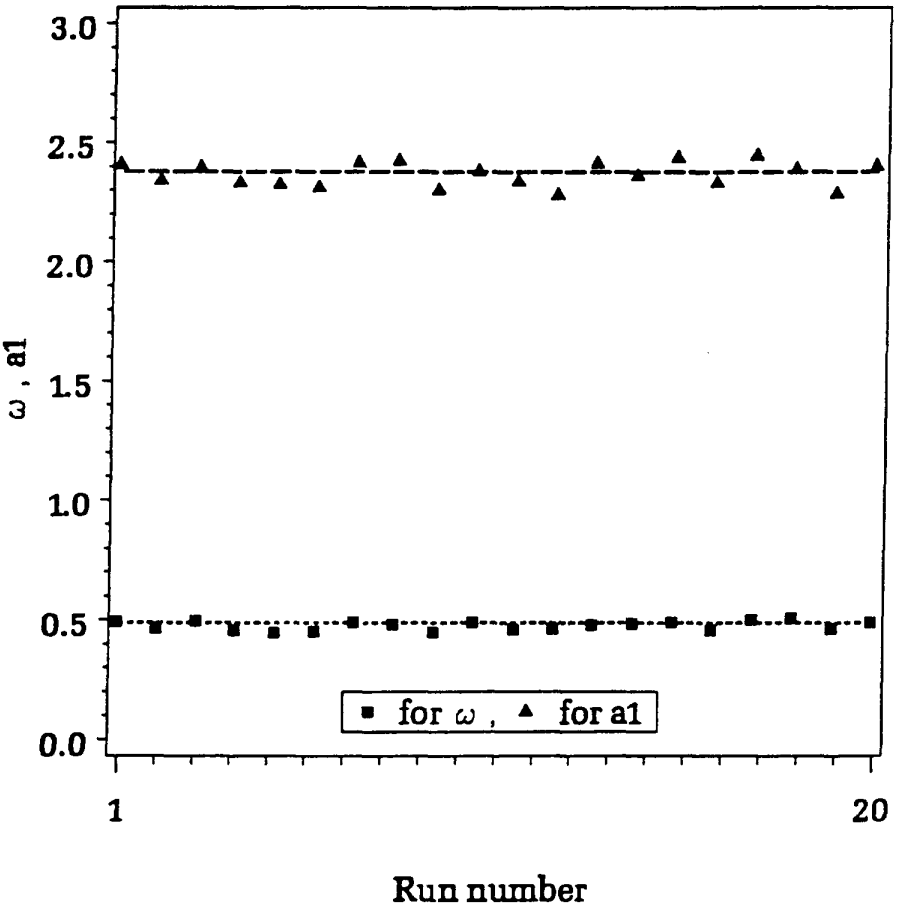

FIGURE 9

Inverse results for the single scattering albedo and the first coefficient of the phase function expansion, and the mean values. The exact values are $\tau_0 = 1.0$, $\omega = 0.5$, and and $a_1 = 2.409$ (PF-1). Random errors are within $\pm 10\%$ for $Q(0)$ and $\pm 5\%$ for $Q(1)$. Converged values without error are $\omega = 0.492$ and $a_1 = 2.394$. The upper bounds are ± 0.040 for $\hat{\omega}$ and ± 0.453 for $\hat{a}_1$.

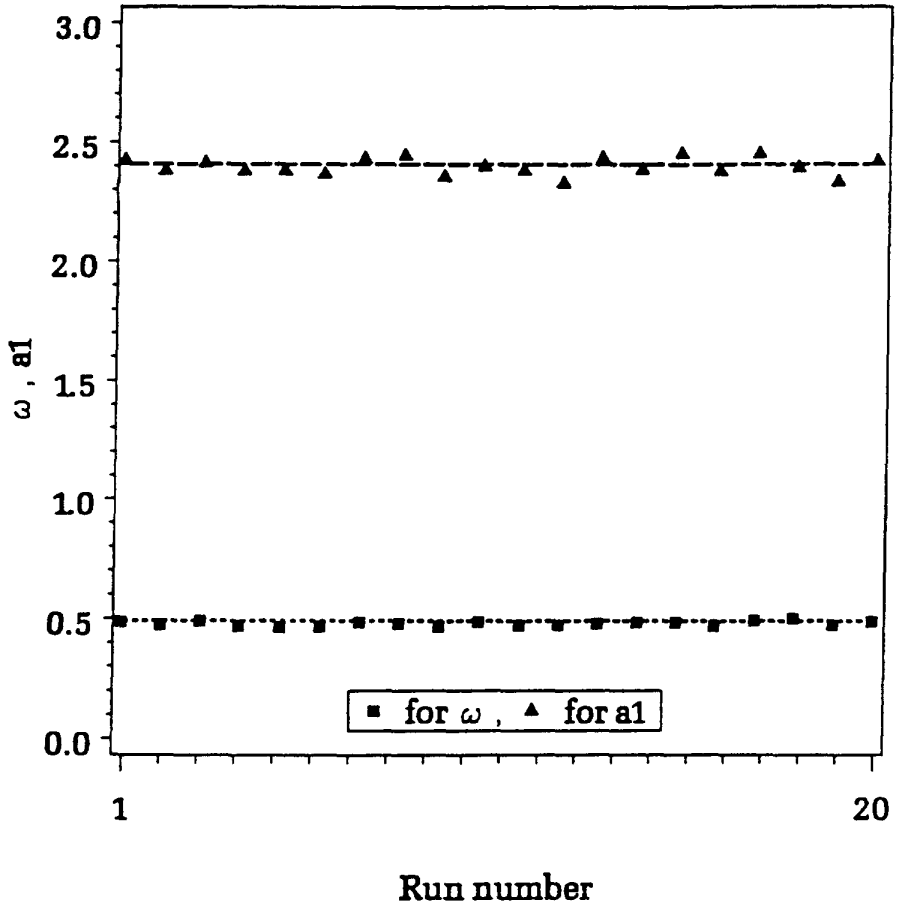

FIGURE 10

Inverse results for the single scattering albedo and the first coefficient of the phase function expansion, and the mean values. The exact values are $\tau_0 = 2.0$, $\omega = 0.5$, and and $a_1 = 2.409$ (PF-1). Random errors are within $\pm 10\%$ for $Q(0)$ and $\pm 5\%$ for $Q(1)$. Converged values without error are $\omega = 0.493$ and $a_1 = 2.420$. The upper bounds are ± 0.017 for $\hat{\omega}$ and ± 0.169 for $\hat{a}_1$.

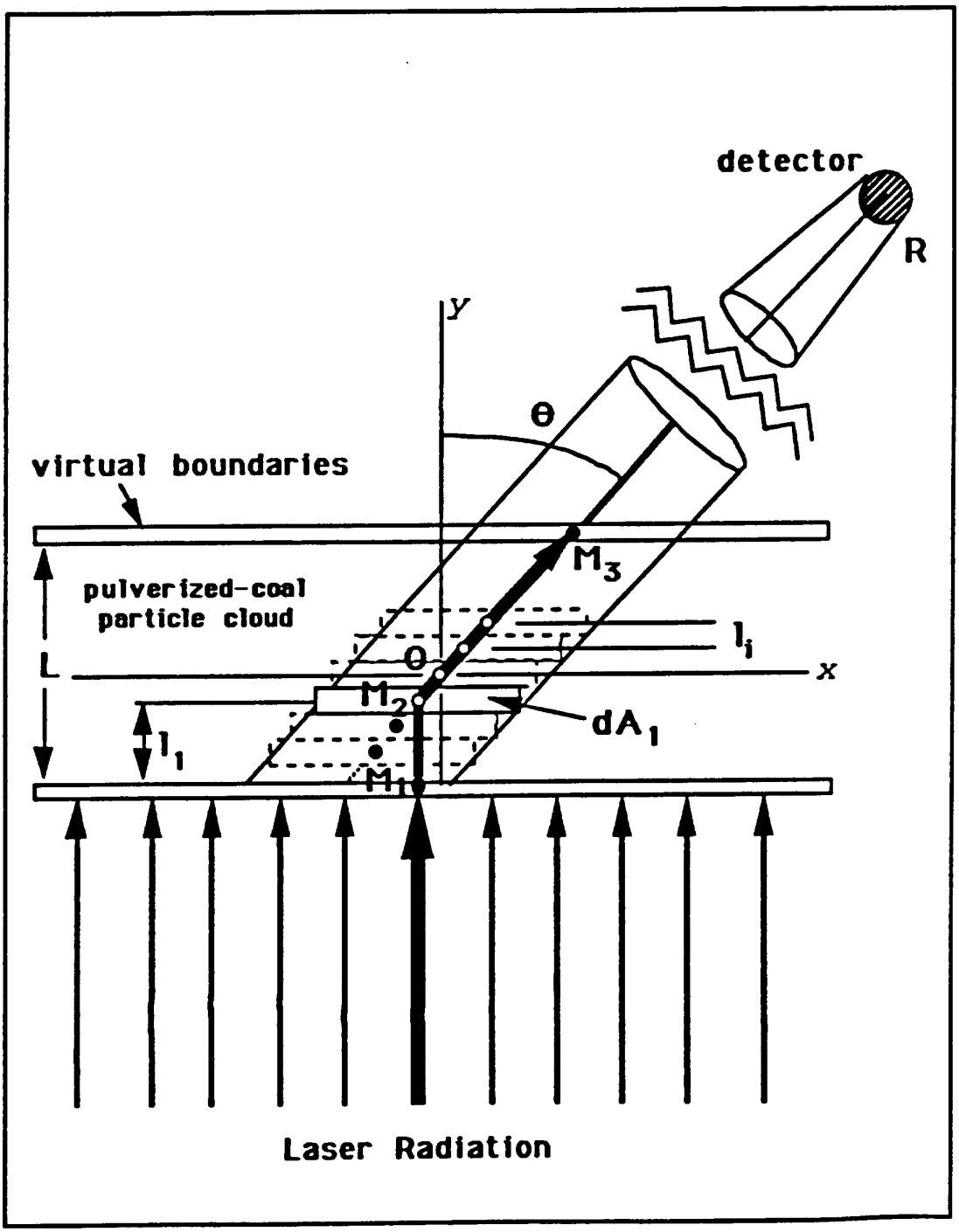

Figure 11 Schematic drawing and nomenclature for first order analytical scattering model.

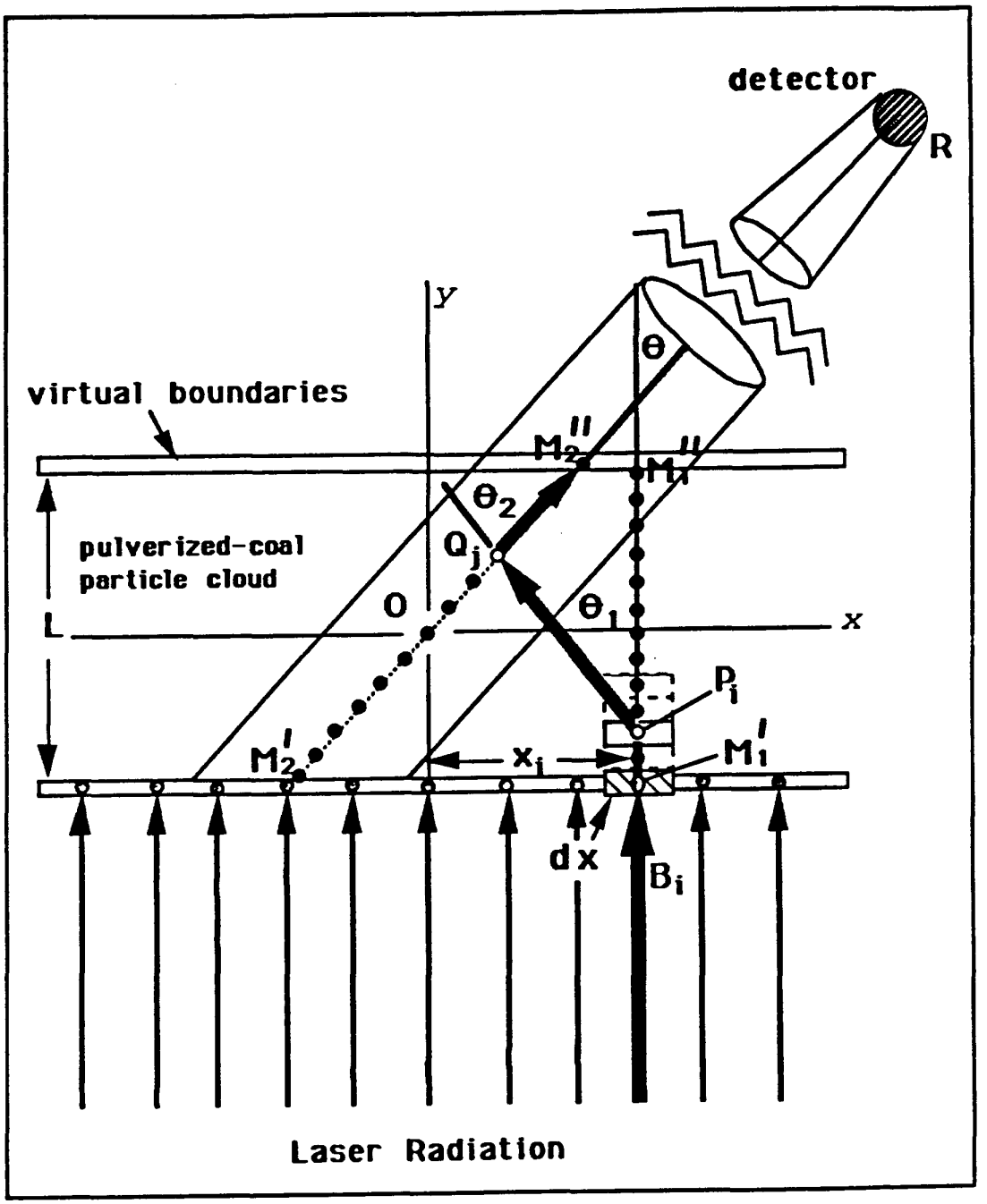

Figure 12 Schematic drawing and nomenclature for second order analytical scattering model.

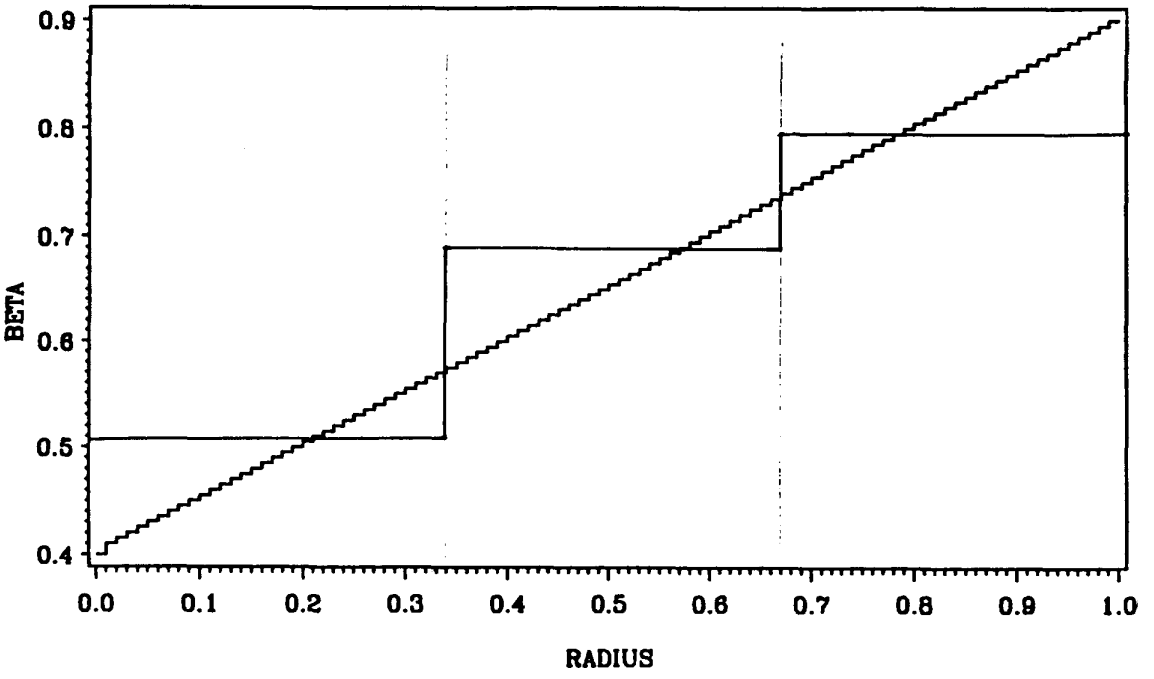

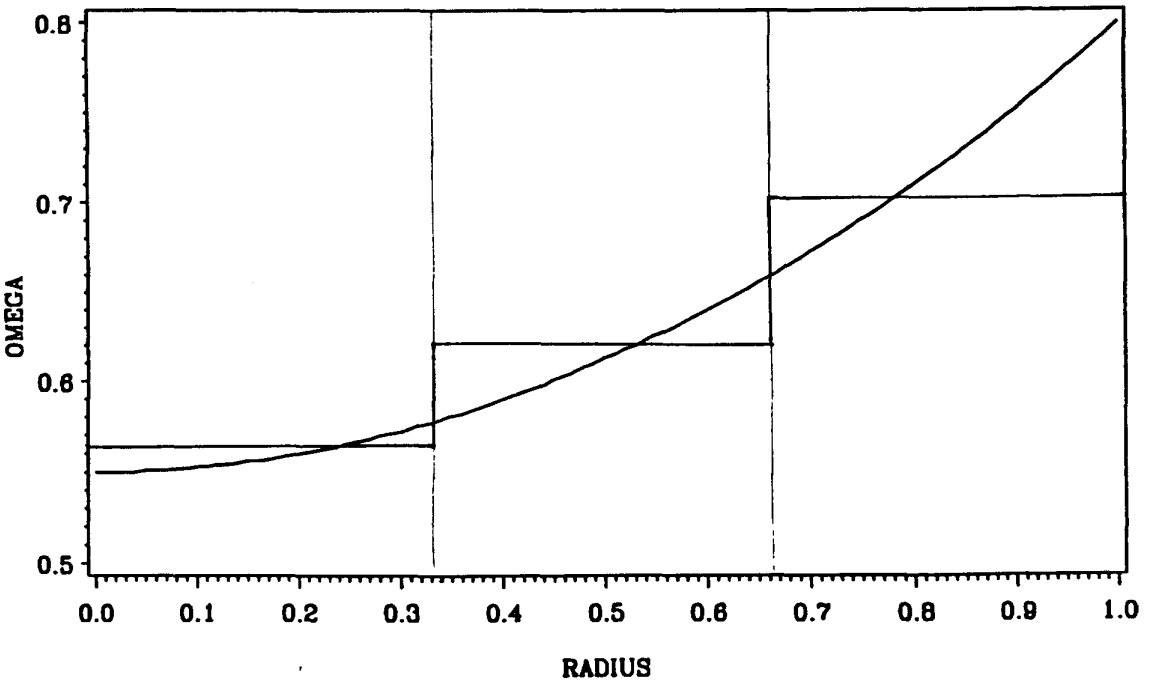

FIGURE 13

Exact and the recovered (three-step) profiles from numerical inversion technique. a) Extinction coefficient distribution; b) Single scattering albedo distribution. $\tau_o = 0.8$; isotropic scattering.

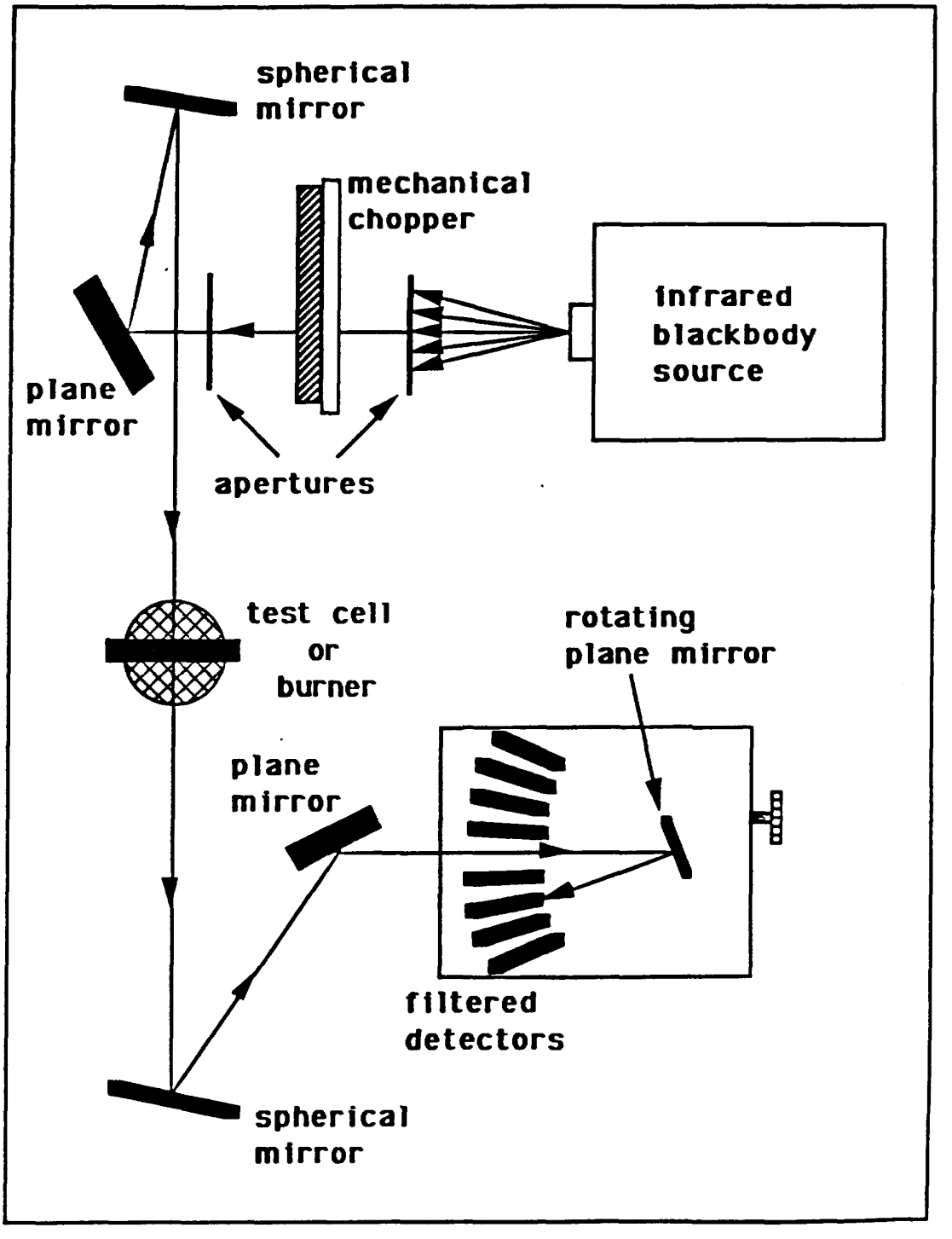

Figure 14 Plan view of multiple-wavelength optical pyrometer.

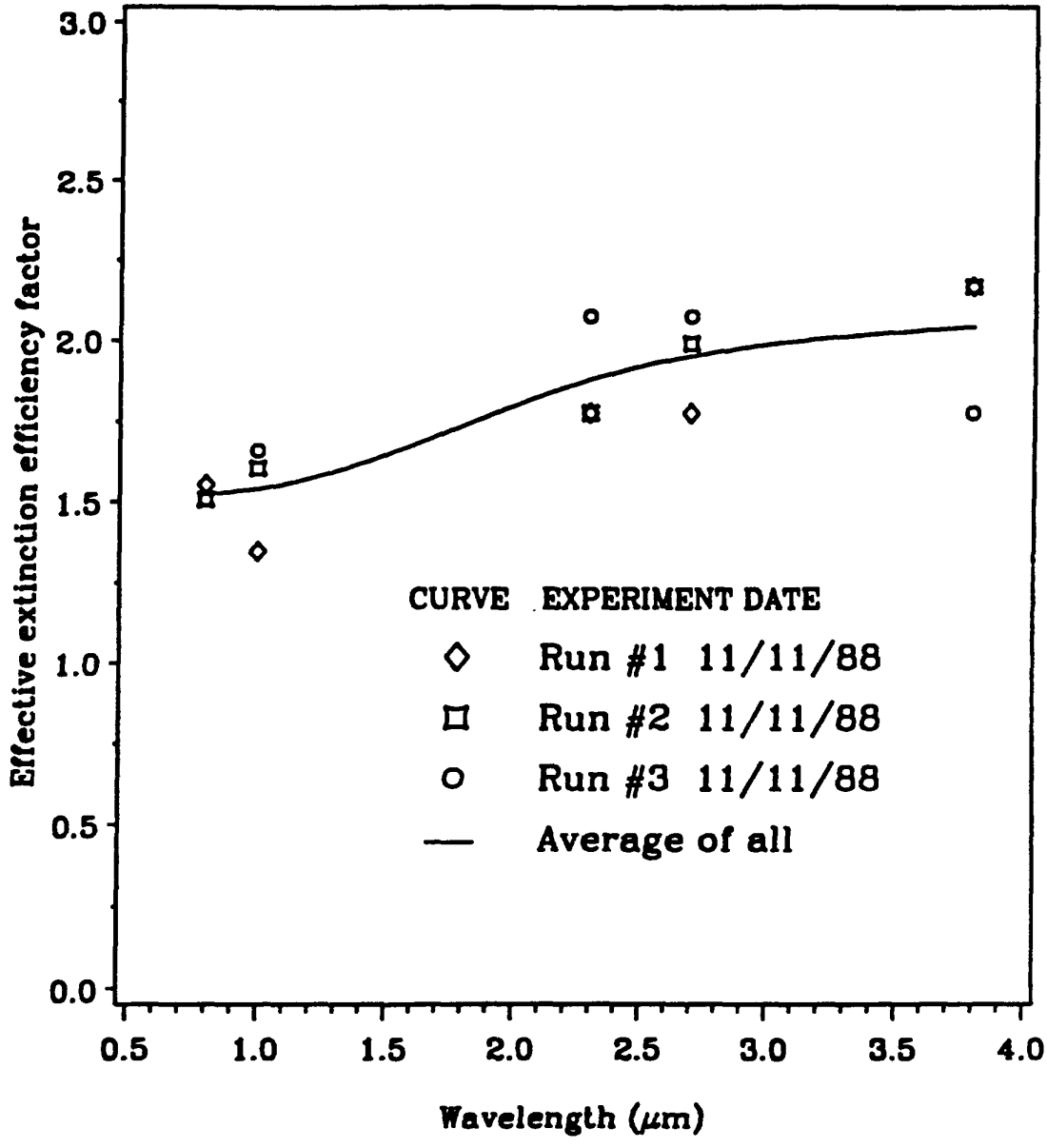

FIGURE 15

Plot of "effective" extinction efficiency factor vs. wavelength for three different experimental runs on 11/11/88.

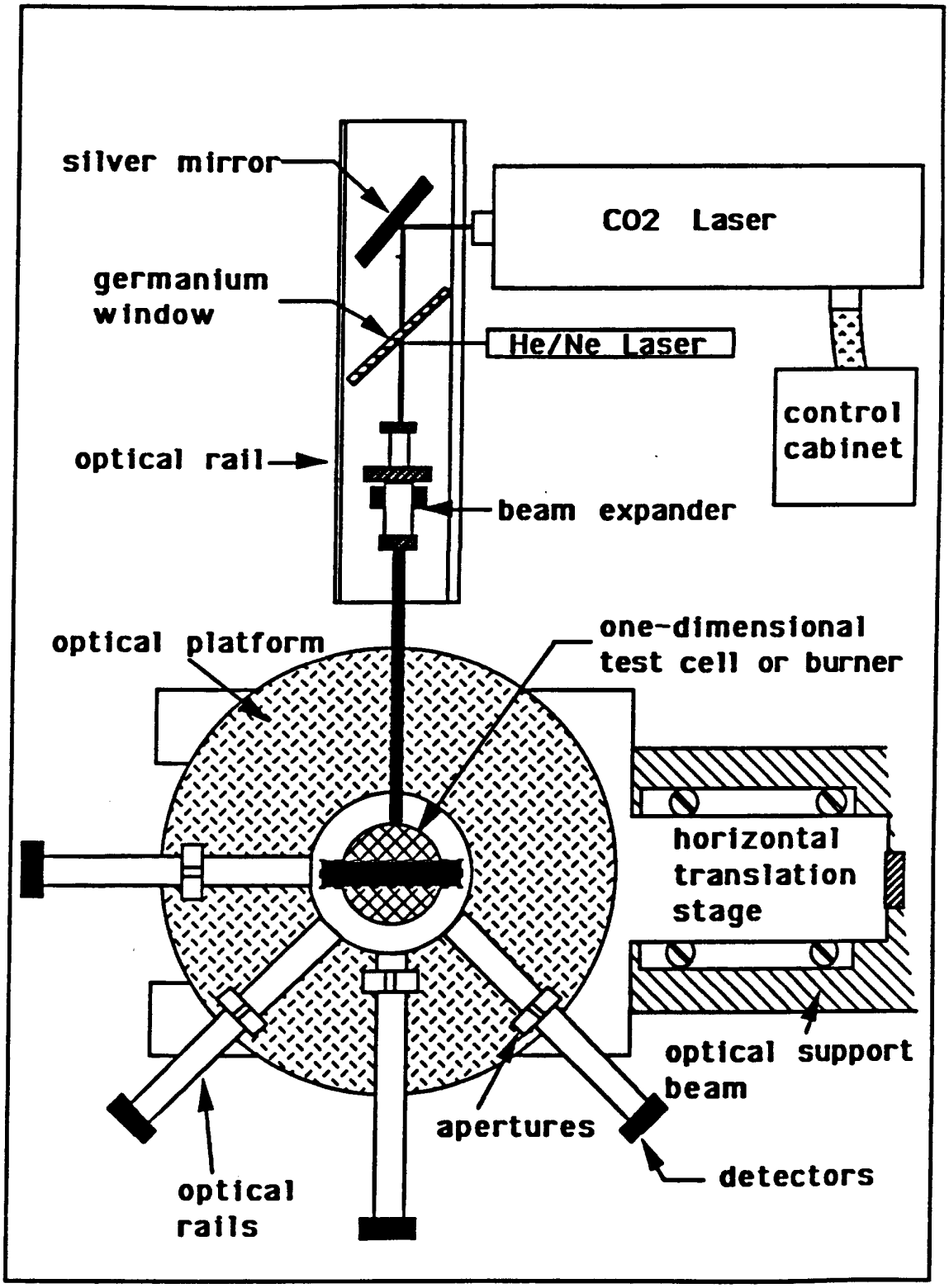

Figure 16 Plan view of the CO_2-laser nephelometer

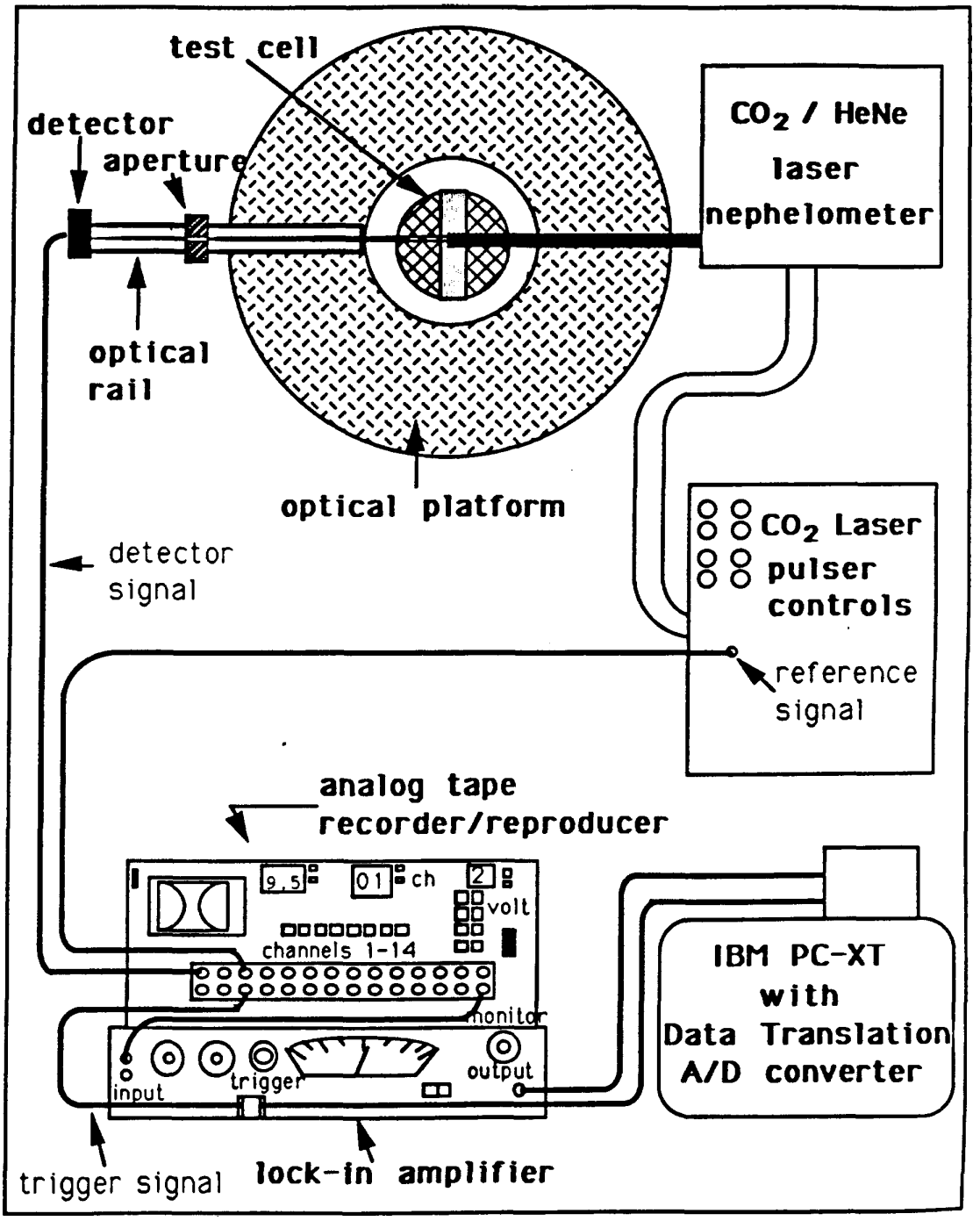

FIGURE 17

Schematic drawing of optical platform and data acquisition system.

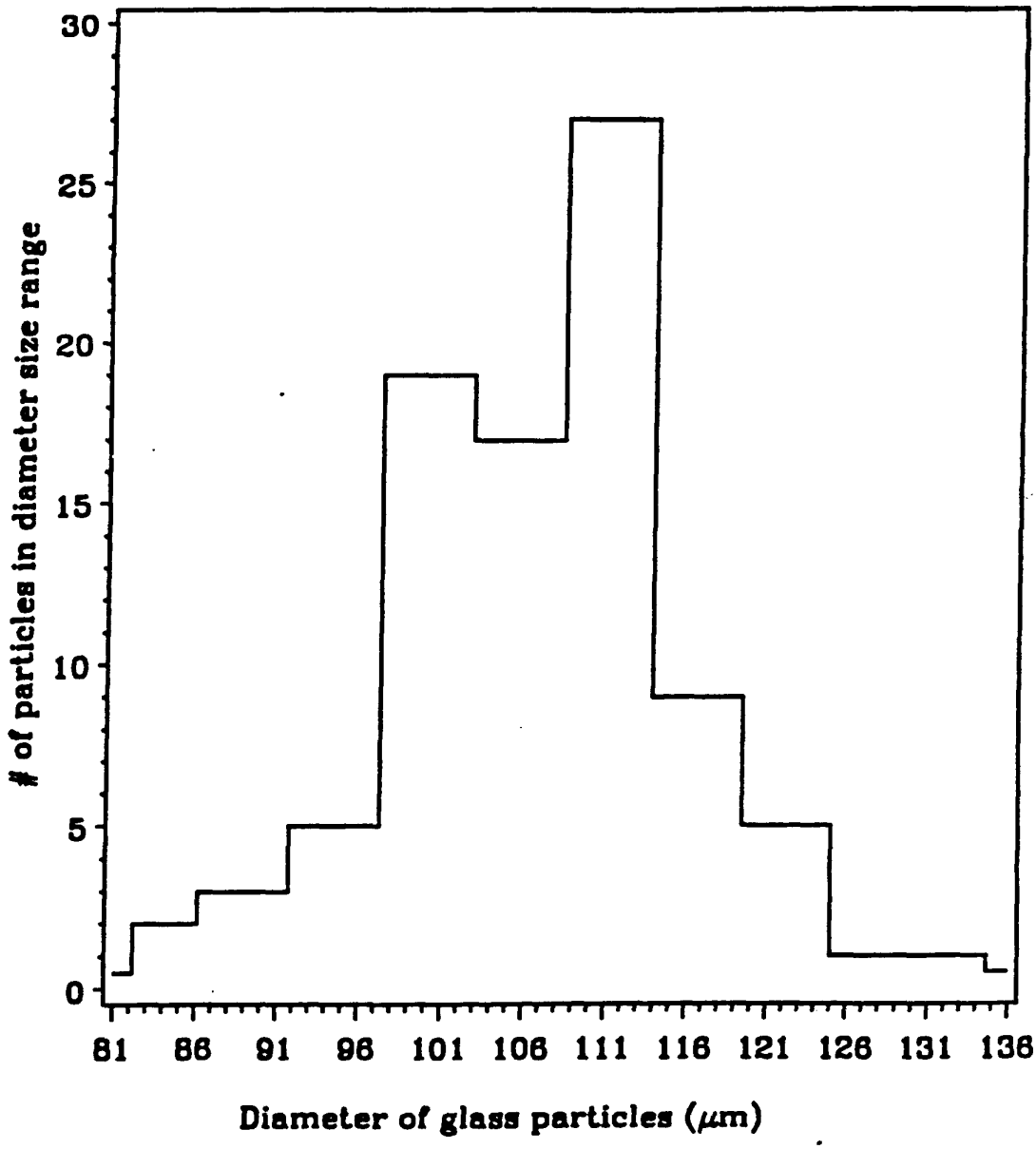

FIGURE 18

Plot of the size distribution function for the glass particles; $D_{86} = 102\mu m$

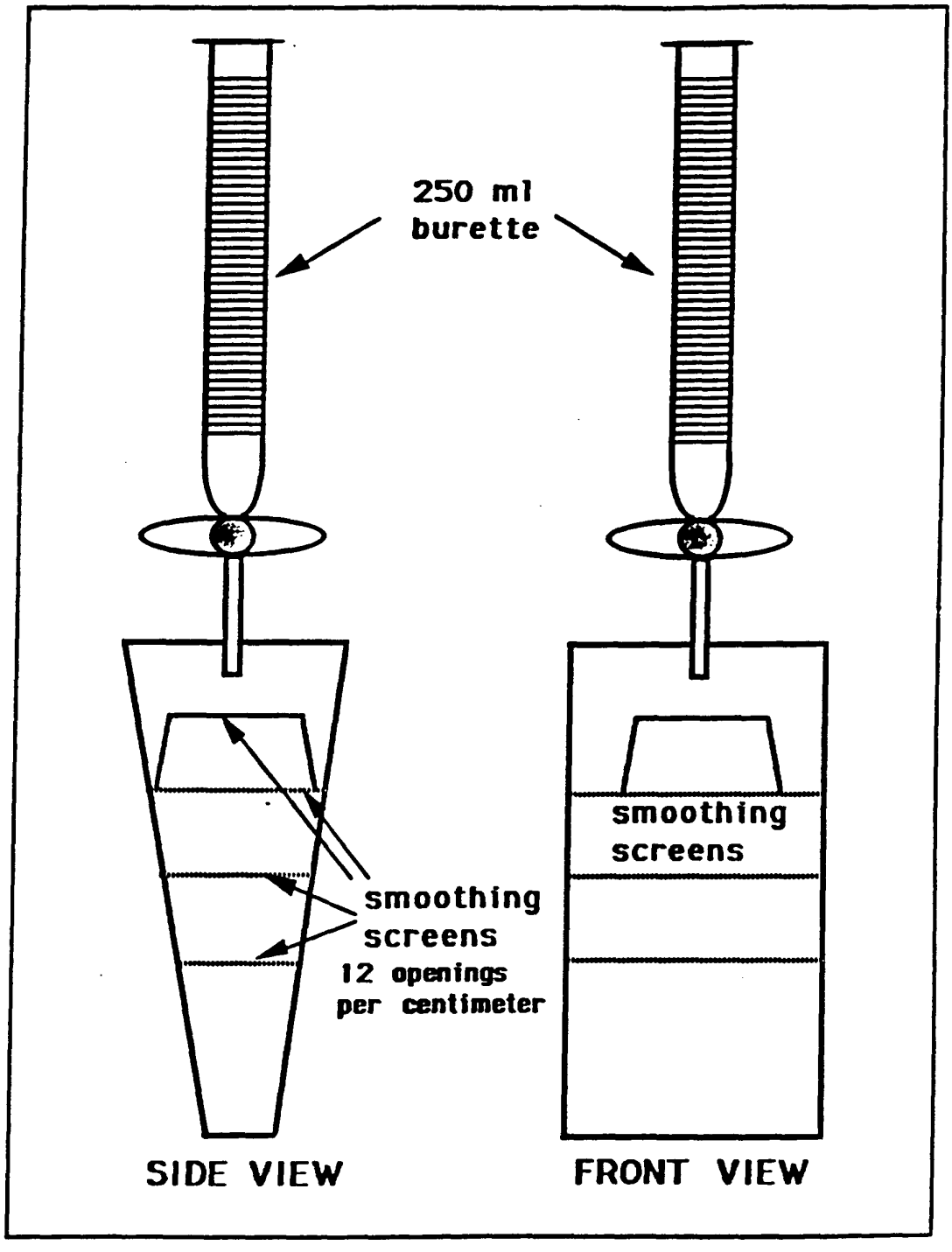

FIGURE 19

Schematic drawing of one-dimensional test cell for glass-particle calibration system.

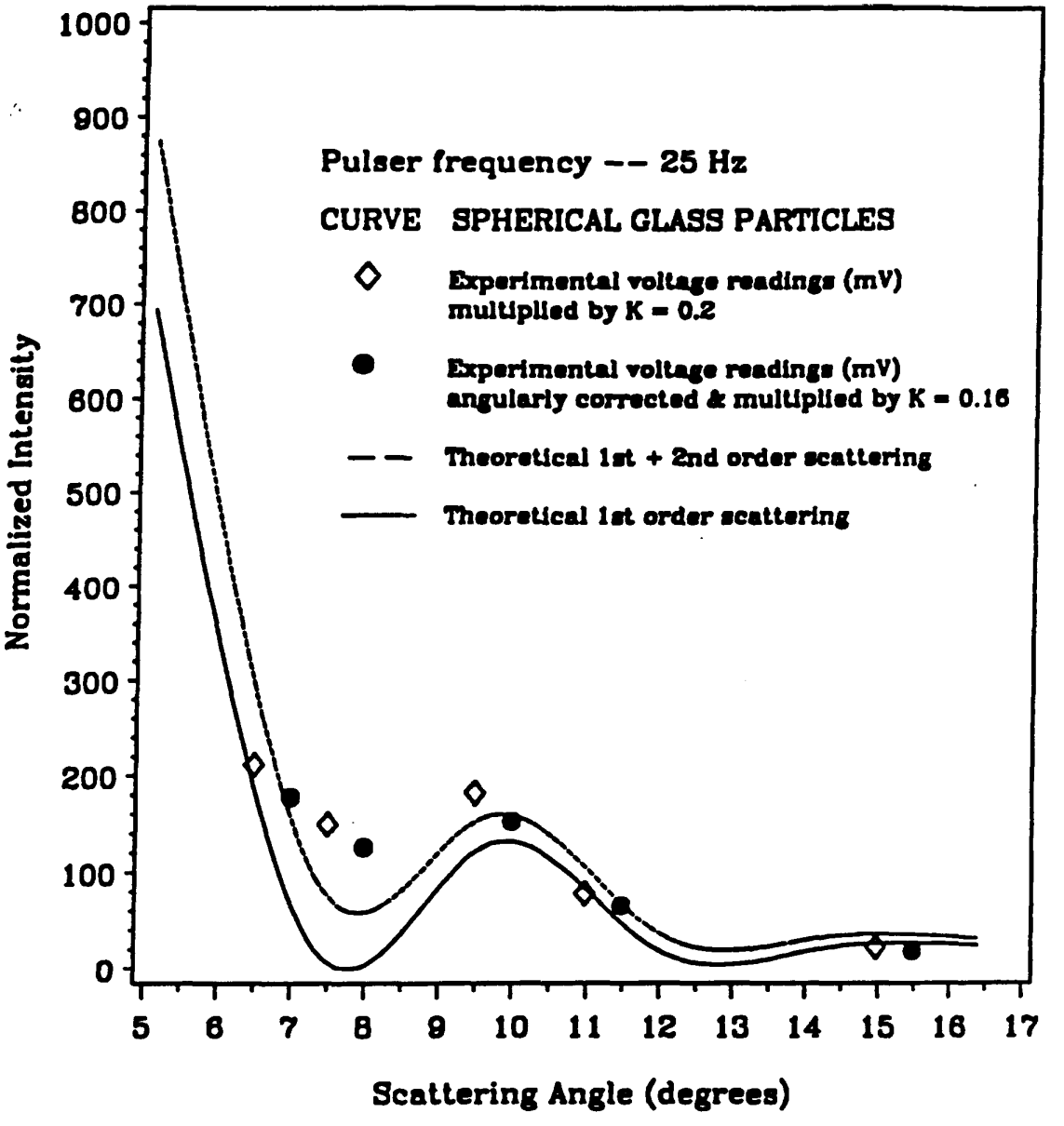

FIGURE 20

Plot of normalized intensity distribution vs. scattering angle comparing the theoretical first and second order scattering with the "effective" experimental voltage values (mV) for the glass particles

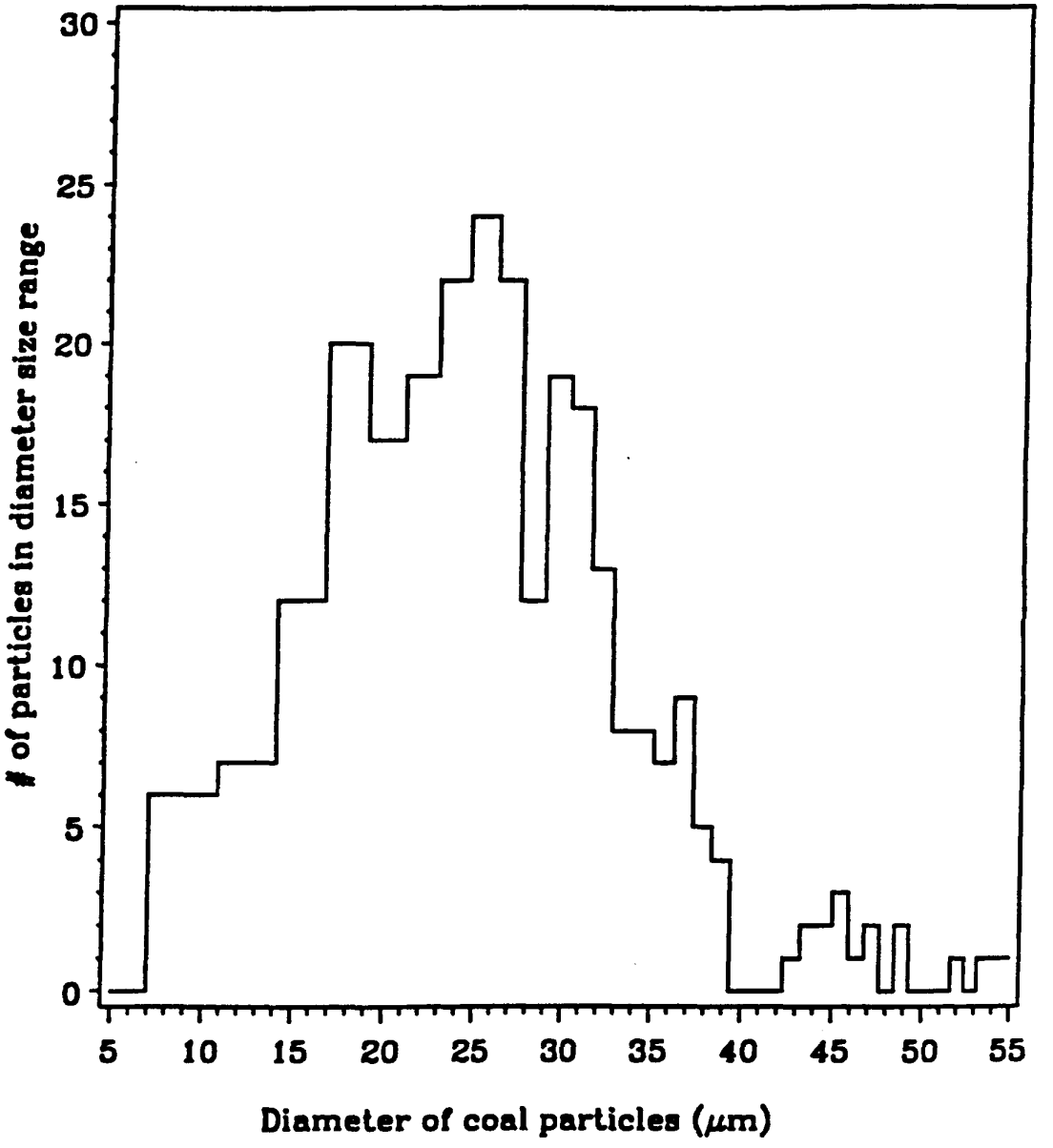

FIGURE 21

Plot of the size distribution function for the smaller size range of pulverized-coal particles.

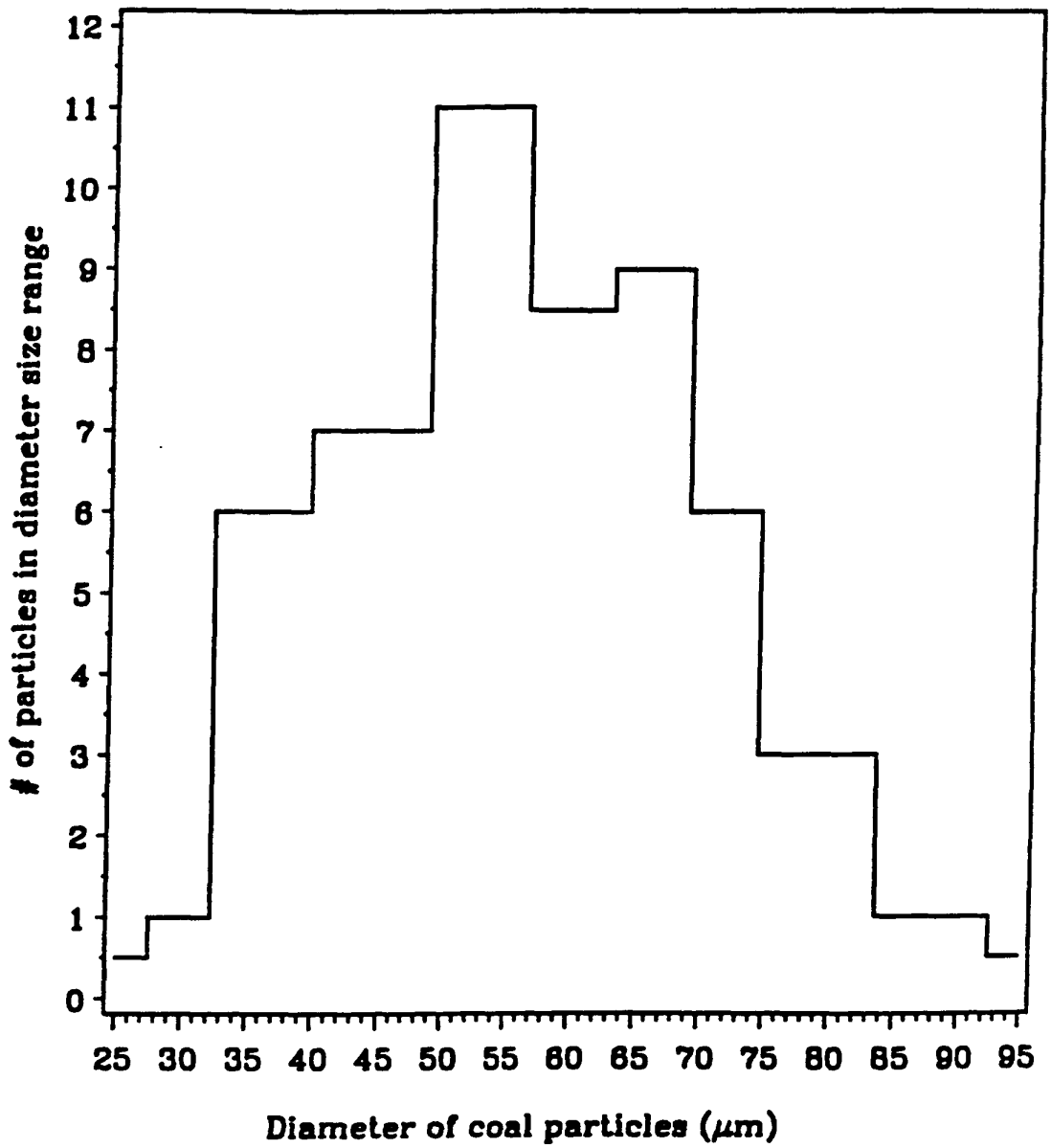

FIGURE 22

Plot of the size distribution function for the larger size range of pulverized-coal particles.

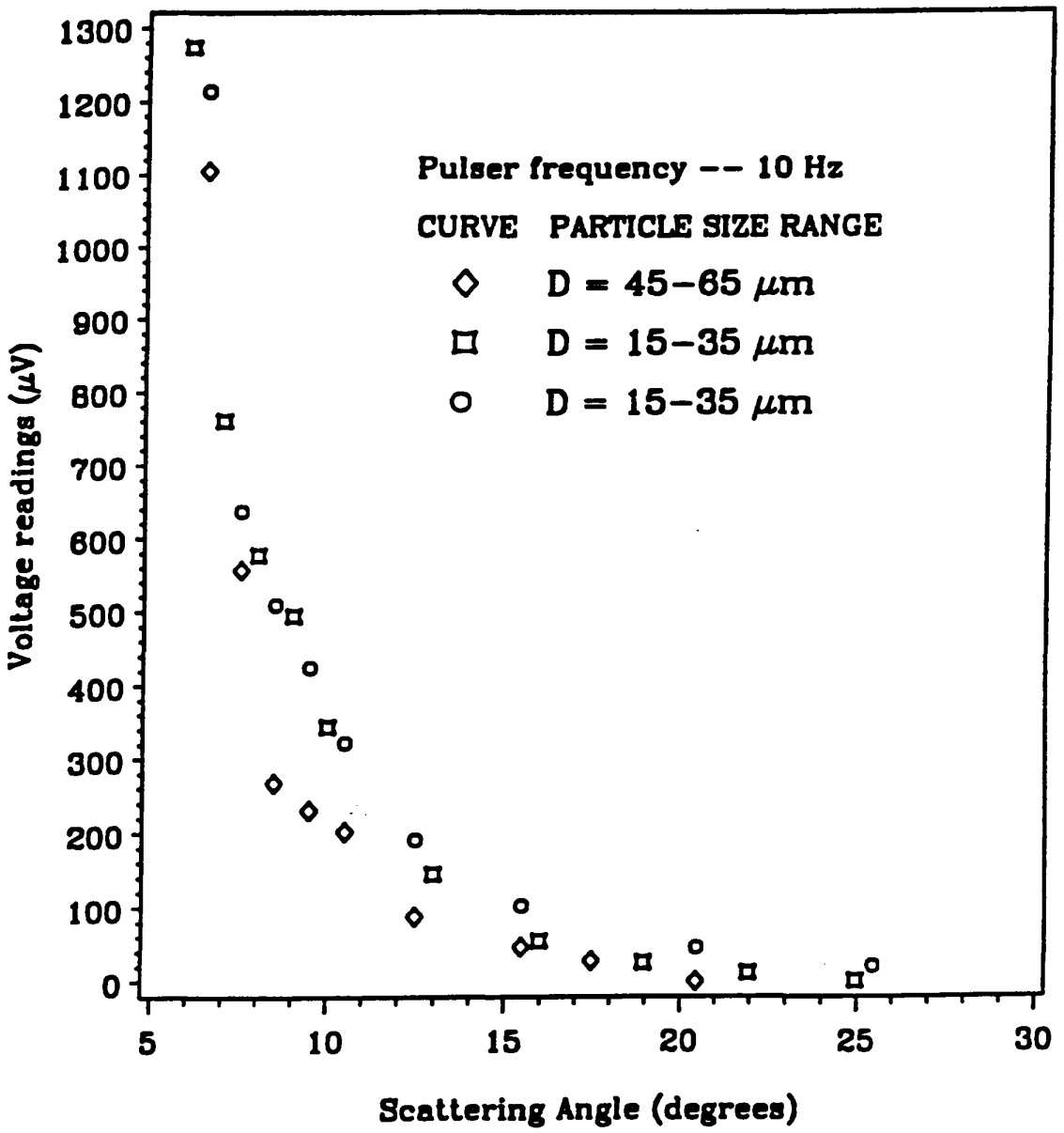

FIGURE 23

Plot of experimental voltage readings vs. scattering angle for the one-dimensional, planar, cold coal-flow system including both size distributions.

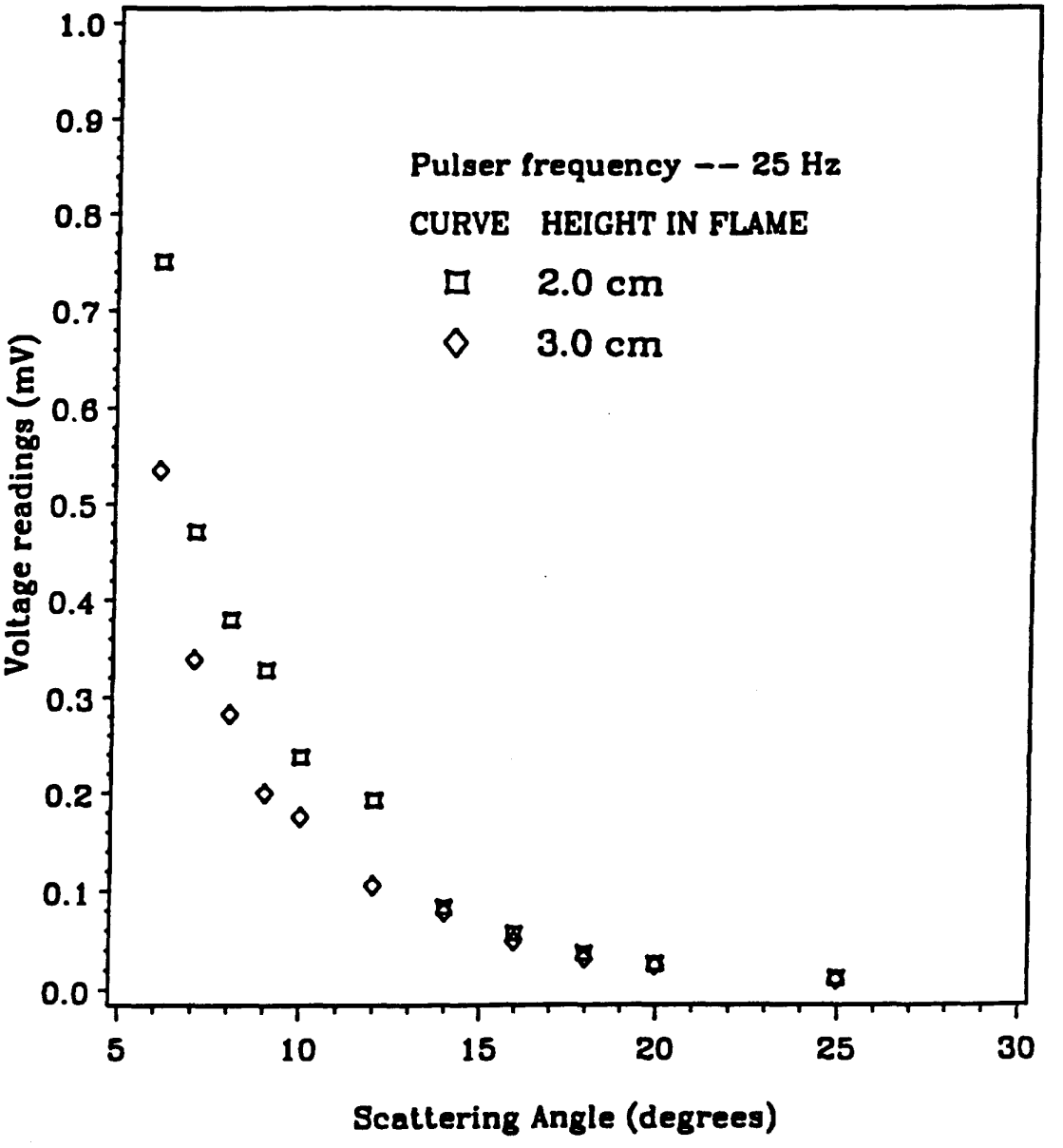

FIGURE 24

Plot of "effective" experimental voltage readings vs. scattering angle